Angular Optical Trapping to Directly Measure DNA Torsional Mechanics

Xiang Gao[1,2], James T. Inman[1,2], and Michelle D. Wang[1,2,*]

[1]Howard Hughes Medical Institute, Cornell University, Ithaca, NY 14853, USA.

[2]Department of Physics & Laboratory of Atomic and Solid State Physics (LASSP), Cornell University, Ithaca, NY 14853, USA.

*Correspondence: mwang@physics.cornell.edu.

Running title: Angular Optical Trapping for Direct Torque Detection

Keywords: angular optical trapping, torque detection, twist, rotation, DNA supercoiling, torsional mechanics, constant-force method, constant-extension method

Abstract

Angular optical trapping (AOT) is a powerful technique that permits direct angular manipulation of a trapped particle with simultaneous measurement of torque and rotation, while also retaining the capabilities of position and force detection. This technique provides unique approaches to investigate the torsional properties of nucleic acids and DNA-protein complexes, as well as impacts of torsional stress on fundamental biological processes, such as transcription and replication. Here we describe the principle, construction, and calibration of the AOT in detail, and provide a guide to the performance of single-molecule torque measurements on DNA molecules. We include the constant-force method, and notably, a new

constant-extension method that enables measurement of the twist persistence length of both extended DNA, under an extremely low force, and plectonemic DNA. This chapter can assist in the implementation and application of this technique for general researchers in the single-molecule field.

1 Introduction

The right-handed helical nature of DNA inevitably results in a highly complex and dynamic DNA topology. During fundamental processes, such as transcription and replication, DNA motor proteins track the helical groove of DNA and thus rotate relative to the DNA. As a result, the DNA may become overwound or underwound, resulting in (+) or (−) DNA supercoiling, respectively [1-7]. DNA supercoiling and resulting torsional stress have been found to be broadly present genome wide [8-10]. However, our understanding of DNA torsional properties has encountered significant experimental challenges.

A complete understanding of DNA torsional mechanics requires knowledge of both the degree of DNA supercoiling and the torque required to supercoil DNA. DNA supercoiling characterizes any additional turns added to DNA, whereas torque characterizes how difficult it is to add those additional turns. Although DNA supercoiling can be assessed by one- and two-dimensional gel electrophoresis, these methods can only measure DNA supercoiling and are unable to measure torque. Conventional optical traps are commonly used to measure force and position of motor proteins and protein-nucleic acid interactions [11-19], but do not have the capacity to measure DNA supercoiling and torque.

To enable direct measurements of both DNA supercoiling and torque, we have developed the angular optical trap (AOT), which adds an entirely new dimension to conventional optical traps [20,21] (Fig. 1). The basic operational principle of the AOT is briefly explained here and will be further explained in detail in subsequent sections. There are three core features of an AOT [22]: birefringent cylinder as the trapping particle, control of the cylinder orientation, and detection of the torque on the cylinder (Fig. 2). In brief, the trapping particle is typically a nanofabricated quartz cylinder, instead of the dielectric microspheres used in a conventional optical trap. Quartz is optically birefringent, with its extraordinary axis more polarizable than its two ordinary axes. The cylinder is fabricated so that its extraordinary axis is perpendicular to the cylinder axis and has one of its ends chemically derivatized for attachment to a biological molecule of interest. Once trapped, the cylinder orients its cylindrical axis along the direction of light propagation due to shape anisotropy and aligns its extraordinary axis with the laser polarization due to optical anisotropy. The cylinder may then be rotated via rotation

of the linear polarization of the incoming trapping laser beam. The torque on the cylinder is detected via the polarization state of the transmitted beam.

Thus, an AOT can control and measure four physical parameters of DNA: torque, rotation (or DNA supercoiling), force, and extension, allowing for a comprehensive examination of the DNA substrate. An AOT has been used to measure the torques required to denature DNA and create different phases [21,23-26], to migrate a Holliday junction [27], to destabilize histone-DNA interactions in a nucleosome [28], to twist single and braided chromatin fibers [29], and to stall RNA polymerase [30,31].

In this chapter, we provide detailed methods and discussion on the construction and calibration of an AOT instrument including the fabrication of quartz cylinders, force and extension measurement, laser polarization rotation, and torque detection. We demonstrate the utility of this instrument by making direct measurements of the torsional persistence lengths of stretched and plectonemic DNA using our newly developed constant-extension method that allows measurements of DNA torsional parameters previously unattainable. We anticipate that this method should be broadly applicable to many studies of DNA torsional mechanics.

1.1 Glossary of Mathematical Symbols

The mathematical symbols are listed in an order that they appear in this chapter.

z_{DNA}: DNA extension, defined as the end-to-end displacement of a DNA molecule.

h_{trap}: trap height, defined as the axial distance between the bottom surface of an untethered cylinder located at the trap center and the top surface of the coverslip.

F: stretching force exerted on the DNA.

k_z: trap stiffness along the direction of light propagation.

z_{cyl}: axial displacement of the cylinder from the trap center.

f_{s}: focal shift ratio to convert piezo movement into trap height change.

ζ: axial displacement signal.

V_{sum}: sum signal of the quadrant photodiode.

P_{P} and P_{S}: laser powers determined by the P and S photodetectors of the input polarization ellipticity detector, respectively.

P: total laser power determined by the input polarization ellipticity detector: $P = P_{\mathrm{P}} + P_{\mathrm{S}}$.

G_{quad}: normalizing factor of the axial displacement signal ζ so that $\zeta = 0$ for an empty trap.

ζ_0: axial displacement signal baseline obtained with a cylinder under no external force.

$\Delta\zeta$: axial displacement signal change: $\Delta\zeta = \zeta - \zeta_0$.

S_z: axial displacement sensitivity: $S_z = \frac{-\Delta\zeta}{z_{\mathrm{cyl}}}$.

z_{p0}: piezo position corresponding to $h_{\mathrm{trap}} = 0$ of a trapped cylinder.

λ_0: laser wavelength in vacuum.

n_{w}: refractive index of the aqueous solution at 1064 nm.

kT: thermal energy.

$\tilde{z}_{\mathrm{cyl}}(f)$: Fourier transformation of z_{cyl}.

β: axial viscous damping coefficient of a cylinder.

$\Gamma(t)$: stochastic force with a Gaussian white noise spectrum.

f_0: corner frequency: $f_0 = \frac{k_z}{2\pi\beta}$.

Θ: polarization angle.

$\Delta\varphi$: phase difference of the light modulated by AOM (P) and AOM (S).

V_A and V_B: A and B photodetector signals in input polarization angle detector, respectively.

χ_{e} and χ_{o}: components of electric susceptibility along extraordinary axis and ordinary axes, respectively.

θ: angle between the electric field of input linear polarized light and the extraordinary axis of a cylinder.

τ_0: maximum optical torque on a cylinder.

P_{R} and P_{L}: powers of the right-handed and left-handed circularly polarized light, respectively.

V_{R} and V_{L}: R and L photodetector signals of the torque detector.

V_{τ}: torque detector signal: $V_{\tau} = V_{\mathrm{R}} - V_{\mathrm{L}}$.

$V_{\tau 0}$: maximum value of the torque detector signal.

V_{τ}': V_{τ} normalized by the total power at the detector: $V_{\tau}' = \frac{V_{\mathrm{R}} - V_{\mathrm{L}}}{V_{\mathrm{R}} + V_{\mathrm{L}}}$.

$V_{\tau 0}'$: $V_{\tau 0}$ normalized by the total power at the detector: $V_{\tau 0}' = \frac{V_{\tau 0}}{V_{\mathrm{R}} + V_{\mathrm{L}}}$.

S_{θ}: angular sensitivity of the torque detector.

$\tilde{\theta}(f)$: Fourier transformation of θ.

k_{θ}: angular trap stiffness.

$C_{\mathrm{eff}}(F)$: effective twist persistence length of an extended DNA molecule, which is force dependent.

C: intrinsic twist persistence length of an extended DNA molecule.

P: twist persistence length of a plectonemic DNA molecule.

2 Materials

2.1 General Components of an AOT

- Trapping laser: CW, linear polarized, diode-pumped solid state (DPSS) laser (J-20-BL10-106C, Spectra-Physics, USA).
- Acousto-optic modulator (Intra-Action, AOM-40R) with a digital frequency synthesizer card (Intra-Action, DVE-120) and a dual RF power amplifier (Intra-Action, DPA 504).
- Beam TAP (Ophir-Spiricon, USA).
- TE200 inverted microscope (Nikon).
- Trapping objective: 100x 1.3 NA, oil immersion, PlanFluor (Nikon).
- Condenser: 60x, 1.4 NA, oil immersion (Nikon).
- Piezo-Stage: P-733.3DD XYZ Piezo Nanopositioner (Physik Instrumente).
- Piezo-Stage Controller: E-727-3CDAP Digital Multi-Channel Piezo Controller (Physik Instrumente).
- LabVIEW VIs for instrument control, data acquisition, and data analysis.

2.2 Cylinder Fabrication

- Wafer: X-cut single-crystal quartz wafer (Precision Micro-Optics).
- Photoresist: OIR-620-7i photoresist.
- I-line, 365-nm GCA stepper tool.
- 3-aminopropyltriethoxysilane (APTES, Sigma-Aldrich).
- Xhric-16 antireflection coating.
- Phosphate-buffered saline (PBS) buffer: 137 mM NaCl, 2.7 mM KCl, 10 mM Na_2HPO_4, 1.8 mM KH_2PO_4.
- O-ring cap tubes (USA Scientific #1415-9710).
- Glutaraldehyde (25% solution, G5882, Sigma-Aldrich)
- Ethanolamine (411000, Sigma-Aldrich).
- Streptavidin protein (SA10, Agilent, formerly Prozyme).
- Acetylated BSA (AcBSA) (AM2614, Thermo Fisher Scientific).

2.3 DNA Sample and Chamber Preparation

- h5α competent cells (#C2978H, New England Biolabs).
- Zymoclean Gel DNA Recovery Kit (D4007, Zymo Research).
- pUC-19 plasmid (New England Biolabs).
- pUC-57 plasmid (Genscript).
- Biotin-14-dATP (19524016, Thermo Fisher Scientific).
- Digoxigenin-11-dUTP (11093088910, Sigma-Aldrich).
- BglI, BstXI and T4 ligase (New England Biolabs).
- β-casein (C6905, Sigma-Aldrich).
- Glass slide (12-550-10, Fisher Scientific).
- Cover glass (12544BP, Fisher Scientific).
- High vacuum grease (Dow Corning).
- Anti-digoxigenin (MB-7000-1, Vector Laboratories).
- ATP (11140965001, Sigma Aldrich).

3 Methods

3.1 Cylinder Fabrication and Coating

In biophysical single-molecule studies, the molecule of interest (for example, DNA) is tethered to a micron-sized particle to be directly manipulated by optical tweezers. A conventional optical trap uses isotropic polystyrene or silica beads, whereas in an AOT, particles made from birefringent material, such as quartz, are used so they can be angularly confined and manipulated [20]. Though micron-sized quartz fragments have been previously used for torque generation, large heterogeneity in shape, size, and orientation of the extraordinary axis of such fragments complicates precise torque measurements [20,32]. Our lab designed and nanofabricated quartz cylinders with high homogeneity, and used these cylinders in single-molecule torque measurements [21]. We made the cylindrical axis perpendicular to the extraordinary axis of the quartz crystal and covalently coat one end of each cylinder with streptavidin for attachment to a DNA molecule labeled with biotin. Due to its shape anisotropy, the cylindrical particle can be optically trapped with its cylinder axis aligned with the direction of laser propagation, so the cylinder can only rotate about the cylindrical axis. This rotation is then confined by the linearly polarized electric field of the trapping laser beam via optical anisotropy. Thus, in this design, the three Euler angles are confined via a combination of optical anisotropy and shape anisotropy to achieve stable angular trapping.

3.1.1 Fabrication Protocol

We have established a detailed nanofabrication method for quartz microcylinders [21] (also see Note 1). For completeness of this chapter, we have repeated the protocol below (Fig. 3A):

1. A 100 mm, x-cut single-crystal quartz wafer is cleaned with hot piranha treatment.
2. Brewer Xhric-16 antireflection coating is spun onto the reverse side of the wafer.
    - 2500 rpm for 30 seconds, 500 R/s ramp rate.
    - Bake at 180°C for 2 minutes.
3. The top surface is derivatized by reaction with 3-aminopropyltriethoxysilane (APTES)

- Add the wafer to ~15 mL of a 1% solution of APTES in 95% ethanol (95% ethanol, 5% water, pH to 5.0 using acetic acid).
- Sonicate wafer in the solution for 4 minutes.
- Remove wafer and immerse in a 50-mL dish of 100% ethanol.
- Repeat this rinse 2 times with fresh ethanol each time, sonicating container briefly each time.
- Bake wafer at 115°C for 20 minutes.

4. The 650 nm of OIR-620-7i photoresist is spun onto the top surface of the wafer.
    - 1850 rpm, 30 s, 500 R/s.
    - 90°C prebake for 120 s.
5. The 10X projection UV lithography with an i-line, 365-nm stepper GCA stepper tool is used to pattern ~0.5 µm diameter posts into the photoresist.
    - Bake for 120 s at 115°C following exposure.
    - Develop wafer in 300 MIF.
6. A plasma oxide etch is performed on the substrate.
    - CHF_3 (50 sccm) O_2 (2 sccm), 60 minutes.
    - Care must be taken so that photoresist is not completely etched away. Otherwise, the underlying amine groups will be damaged.
7. Residual resist is removed by 20-minute sonication in acetone (Fig. 3B and C).
8. Cylindrical posts are removed from the wafer (Fig. 3D and E).
    - Gently scrape the surface with a clean razor blade.
    - Collect the powdery product.

3.1.2 Coating Protocol

The nanofabricated cylinders are specifically functionalized with streptavidin at one end (Note 2). The protocol is shown below:

1. Collect the cylinders removed from the wafer into a 1.5 mL centrifuge tube. Add deionized water to a final volume of 1 mL. If needed, remove 5 µL of sample and dilute 10 times with DI water for EM imaging. Centrifuge for 10 minutes at 13,000 rpm (~17,900 x g) in a table-

top microcentrifuge to form a compact white pellet, and then carefully pipette out the supernatant.

2. Wash the cylinders by repeating the following steps twice.
    a. Add fresh PBS to 1 mL. Resuspend the cylinders by vortexing until the white pellet disappears. Then vigorously sonicate the tube for 30 seconds.
    b. Centrifuge for 10 minutes at 13,000 rpm (~17,900 x g) in a table-top microcentrifuge to form a compact white pellet, and then carefully pipette out the supernatant.
3. Activate the cylinders with glutaraldehyde.
    a. Add 700 µL 1.4x PBS. Resuspend the cylinders by vortexing until the white pellet disappears. Then sonicate the tube for 30 seconds.
    b. Thaw glutaraldehyde stock at room temperature (initially stored at -20°C in ampoules). Add 300 µL 25% glutaraldehyde.
    c. Place the tube on a rotator at 40 rpm for 3 hours at room temperature.
    d. Wash the cylinders by repeating step 2 four times.
4. Covalently bind streptavidin to the cylinder.
    a. Add 1 mL PBS with 0.5 mg/mL streptavidin. Resuspend the cylinders by vortexing until the white pellet disappears. Then sonicate the tube for 30 seconds.
    b. Place the tube on a rotator at 40 rpm to react overnight at room temperature.
    c. Wash the cylinders by repeating step 2 one time.
5. Block unreacted sites on the cylinder surfaces.
    a. Add 1 mL PBS with 0.2 M ethanolamine.
    b. Resuspend the cylinders by vortexing until the white pellet disappears. Then sonicate the tube for 30 seconds.
    c. Place the tube on a rotator at 40 rpm for 30 minutes at room temperature.
    d. Wash the cylinders by repeating step 2 twice.
6. Block any remaining non-specific protein binding sites on the cylinder surface with acBSA.
    a. Add 1 mL PBS with 0.1 mg/mL acBSA. Resuspend the cylinders by vortexing until the white pellet disappears. Then sonicate the tube for 30 seconds.
    b. Place the tube on a rotator at 40 rpm for 30 minutes at room temperature.

c. Wash the cylinders by repeating step 2 once.

7. Add 1 mL storage buffer (PBS buffer with 0.1 mg/mL acBSA and 0.05% NaN_3). Resuspend the cylinders by vortexing until the white pellet disappears. Then sonicate the tube for 30 seconds. Store the cylinder suspension in screw-top tubes with an o-ring cap. Seal the tubes with parafilm.

3.2 Sample Preparations

3.2.1 Torsionally Constrained (TC) DNA Sample Preparation

A torsionally constrained template is composed of a single, long DNA sequence of interest with two short flanking DNA adaptors of approximately 500 bp each, with multi-labels (Fig. 4). This DNA sample is created using a method similar to that previously described [21,29]. Briefly:

1. Create a high-copy plasmid by inserting a sequence of interest into pUC19 between BglI and BstXI recognition sites.
2. Transform the plasmid to *E. coli* (h5α competent cells). Amplify and purify the plasmid from *E. coli* according to the manufacturer's instructions.
3. To obtain the DNA of interest, digest the plasmid with BglI and BstXI and purify the DNA by gel extraction.
4. To create the adapters, a 482-bp DNA sequence flanked by BglI and BstXI cutting sites was cloned into pUC57.
5. This adapter sequence is then amplified and labeled by performing two separate polymerase chain reactions (PCRs), one with 25% of dATP replaced by biotin-14-dATP and the other with 25% of dTTP replaced by digoxigenin-11-dUTP.
6. The two PCR products are digested with BglI and BstXI to create overhangs for the biotin- and dig-adaptors, respectively. The final DNA construct is formed via ligation of the DNA sequence of interest with the two multi-labeled adaptors (Fig. 4).

3.2.2 DNA Sample Chamber Preparation

To measure the torsional property of DNA, tether one end of a single DNA molecule to the chamber's bottom surface and the other end to the bottom of a cylinder. We describe in this subsection how to prepare a sample chamber for such an experiment (Fig. 5).

Conventional sample chambers are usually made using double-sided tape. The tape stably composes the side walls of the chamber but can gradually release unknown chemicals which may change the buffer composition over time. Therefore, we designed a new chamber configuration using inert high vacuum grease as the side walls of the chamber. The steps to make a grease chamber are listed below:

1. Fill a 10 mL syringe fitted with a 200 µL pipette tip with high vacuum grease.
2. Clean the coverslip and glass slide with Windex and thoroughly wash them with DI water. Let the coverslip and slide dry completely.
3. Stick two strips of double-sided tape on the coverslip. The distance between the two strips is around 10 mm. Then use the syringe to draw two thin lines of high vacuum grease inside the tape (Fig. 5A, left).
4. Attach a cleaned slide (Fig. 5A, right) on top of the coverslip to form a chamber structure (Fig. 5B).

The steps to tether DNA molecules in the chamber are listed below:

1. Flow 18 µL 0.022 mg/mL anti-digoxigenin in PBS into the grease chamber. Incubate for 10 minutes at room temperature.
2. Flow 60 µL 10 mg/mL β-casein solution into the chamber and incubate for 20 minutes at room temperature. β-casein has been shown to be an effective reagent for surface passivation [33,29].
3. Flush the chamber with 100 µL PBS buffer with 1.0 mg/mL β-casein.
4. Flow 40 µL of 5 pM DNA in PBS with 1.0 mg/mL β-casein into the chamber and incubate for 30 minutes at room temperature.
5. Wash the chamber with 100 µL PBS buffer with 1.0 mg/mL β-casein.
6. Flow 20 µL diluted cylinders (~30 fM), which have been thoroughly resuspended in PBS buffer with 1.0 mg/mL β-casein, into the chamber, and incubate for 30-60 minutes at room temperature.

7. Wash the chamber with 100 µL PBS buffer with 1.0 mg/mL β-casein.
8. Wash the chamber with 100 µL final buffer of interest. Then seal the chamber with high vacuum grease.

3.3 DNA Extension and Force Measurement

In addition to its ability to measure torque and rotation of a cylinder, an AOT can directly measure force and displacement of a trapped cylinder. Because the optical torque is exerted axially (Fig. 1), the natural direction for force application is also along the axial direction. Figure 1 shows an experimental configuration that uses an AOT to measure DNA torsional properties when the DNA is held under force. Here, the DNA is torsionally constrained at one end to the surface of a coverslip and at the other end to the bottom of a trapped cylinder. In such a configuration, DNA may be twisted while being stretched axially.

During this process, the DNA extension z_{DNA} is measured. z_{DNA} is the end-to-end distance of DNA measured between the bottom surface of the cylinder and the top surface of the coverslip (Fig. 6C):

$$z_{\mathrm{DNA}} = h_{\mathrm{trap}} - z_{\mathrm{cyl}}. \qquad \text{Eq. 1}$$

h_{trap} is the trap height, defined here as the axial distance between the bottom surface of an untethered cylinder located at the trap center and the top surface of the coverslip (Fig. 6B). z_{cyl} is the axial displacement of the cylinder from the trap center and is measured by an axial displacement detector (Fig. 6C). In our instrument, the axial stretching of DNA is achieved by modulating h_{trap} via a piezo-electrically controlled sample stage. For small displacements of the cylinder from the trap center, the optical trap acts like a Hookean spring made of light, such that the stretching force exerted on the DNA is proportional to cylinder displacement:

$$F = k_z \cdot z_{\mathrm{cyl}}, \qquad \text{Eq. 2}$$

where k_z is the trap stiffness and is proportional to the input laser power P.

To determine z_{DNA}, it is also critical to accurately determine h_{trap}. This requires knowledge of the piezo position at which $h_{\mathrm{trap}} = 0$. In addition, when an oil immersion objective is used, a change in the piezo position is not equal to a change in the trap height, $\Delta h_{\mathrm{trap}} \neq \Delta z_{\mathrm{piezo}}$, due to the mismatch of the index of refraction at the interface between the

glass coverslip and the aqueous solution of the sample chamber. This requires determination of the focal shift ratio to convert piezo movement into trap height change: $f_{\mathrm{s}} = \Delta h_{\mathrm{trap}}/\Delta z_{\mathrm{piezo}}$.

In this section, we discuss these considerations in detail and outline methods and protocols to address them. This section serves as necessary groundwork for subsequent sections related to torque and rotation.

3.3.1 Detect the Axial Cylinder Displacement z_{cyl}

In an AOT, the axial position detection of a trapped cylinder is performed using the trapping laser via back-focal-plane interferometry [34-36]. This technique exploits the interference of scattered and un-scattered light detected by a quadrant photo detector placed in the back-focal-plane of a condenser. Due to the Gouy-phase shift in a focused beam, the axial displacement of a trapped cylinder from the trap center can be determined. The sensitivity of the axial displacement signal is optimized by tuning the condenser aperture diaphragm [37].

We define the laser-power-normalized axial displacement signal

$$\zeta = 1 - \frac{G_{\mathrm{quad}} \cdot V_{\mathrm{sum}}}{P}, \qquad \text{Eq.3}$$

where V_{sum} is the sum signal of the quadrant photodiode and $P = P_{\mathrm{P}} + P_{\mathrm{S}}$ is the total laser power input to the objective with P_{P} and P_{S} being the laser powers determined by the P and S photodetectors of the input polarization ellipticity detector, respectively. G_{quad} is a normalizing factor and set to a value so that $\zeta = 0$ for an empty trap. G_{quad} is calibrated at the beginning of an experiment using an empty trap. The axial displacement signal baseline ζ_0, the axial displacement signal of a cylinder under no external force, depends on the size and shape of the trapped particle, which may vary slightly from cylinder to cylinder. Thus ζ_0 should be determined for each cylinder.

Under a stretching force, the trapped cylinder will be pulled away from the trap center. The axial displacement signal change, $\Delta\zeta = \zeta - \zeta_0$, linearly decreases with an increase in z_{cyl} for small cylinder displacements (typically < 200 nm). For convenience, we also define a parameter called axial displacement sensitivity $S_z = \frac{-\Delta\zeta}{z_{\mathrm{cyl}}}$, which measures how sensitive the axial displacement signal is to cylinder displacement.

3.3.2 Find the Surface: $h_{\mathrm{trap}} = 0$

To find the piezo position z_{p0} corresponding to $h_{\mathrm{trap}} = 0$ of a trapped cylinder, we move the coverslip towards the cylinder and identify the piezo position at which the trapped cylinder encounters resistance to further movement as it approaches the surface (Fig. 7A). To begin, the trap height is roughly set to a fraction of the DNA tether's contour length such that there is only a very small force on the cylinder. Next, the trap height is decreased by moving the coverslip towards the cylinder via the *z* piezo until the cylinder starts to contact the surface, at which point, ζ starts to increase. Continued movement of the coverslip then carries the cylinder through the trapping laser beam such that the laser beam scans the cylinder, resulting in a peak in ζ. A representative ζ vs. z_{piezo} plot is shown in Fig. 7B. This entire curve is then fit with the following two-piece function composed of a parabola and a line, with their intersection being defined as the surface position (Fig. 7B):

$$\zeta = \begin{cases} A \cdot \left(z_{\mathrm{piezo}} - z_{\mathrm{p0}}\right)^2 + B \cdot \left(z_{\mathrm{piezo}} - z_{\mathrm{p0}}\right) + \zeta_0, z_{\mathrm{piezo}} < z_{\mathrm{p0}} \\ \zeta_0, z_{\mathrm{piezo}} \geq z_{\mathrm{p0}} \end{cases}, \qquad \text{Eq. 4}$$

where ζ_0 is the axial displacement signal baseline, and A and B are fit parameters.

During this process, a low trapping laser power should be used to avoid potential photo-damage to DNA and to minimize cylinder sticking to the surface. However, a low laser power permits a greater amplitude of Brownian motion of the cylinder, leading to a surface contact being detected earlier than desired. Indeed, by comparing the Brownian motion amplitude and the detected surface position at different powers, we found that Brownian motion is predominately responsible for the overestimation (Fig. 7C). Thus, we compensate for this effect by subtracting the Brownian motion amplitude from the measured surface position.

3.3.3 Determine the Focal Shift Ratio

The focal shift ratio depends on several factors including the refractive index mismatch of the glass-aqueous solution interface, the laser beam overfilling of the objective back aperture, and the immersion medium and the numerical aperture of the objective. The focal shift ratio can be measured by several methods, two of which are described below.

The first method takes advantage of the Fabry-Pérot effect that results from laser beam interference [38,36,39] between the cylinder's bottom surface and the sample chamber's top surface (Fig. 8A). The interference can be constructive or destructive, dependent on the trap height. The intensity of this interference can be detected by the axial displacement signal ζ. As shown in a representative curve in Fig. 8B, ζ varies with z_{piezo} in a sinusoidal fashion. The focal shift ratio may be obtained from the period of this curve. To obtain the period of the interference pattern, we fit the curve with an exponentially decaying sinusoidal function with a slope and an intercept:

$$\zeta = a_1 + a_2 \cdot z_{\mathrm{piezo}} + a_3 \cdot \sin\left(2\pi z_{\mathrm{piezo}}/a_4 + a_5\right) \cdot \exp\left(-a_6 \cdot z_{\mathrm{piezo}}\right), \quad \text{Eq.5}$$

where a_1 to a_6 are the fitting parameters with a_4 being the period. Based on the definition of the focal shift ratio, the change of trap height between two constructive peaks should be $f_{\mathrm{s}}a_4$, and it is also equal to half of the wavelength of the laser in the aqueous solution, $\lambda_0/(2n_{\mathrm{w}})$, where λ_0 is the laser wavelength in vacuum, and n_{w} is the refractive index of the aqueous solution. Therefore, the focal shift can be calculated as follows:

$$f_{\mathrm{s}} = \frac{\lambda_0}{2n_{\mathrm{w}}a_4}. \quad \text{Eq.6}$$

Below are detailed steps for this method:

1. Make a sample chamber containing cylinders suspended in PBS buffer. Seal the chamber with high vacuum grease.
2. Set the laser power to 100 mW. This is a rather high laser power that can generate a stiff trap to suppress the Brownian motion of the cylinder, minimizing the noise in the measurement.
3. Trap a cylinder, and then move the *z* piezo up until the cylinder contacts the coverslip of the sample chamber.
4. Move the *z* piezo down slowly and record ζ.
5. Fit the result to obtain the focal shift ratio.
6. Repeat the experiment on 20 different cylinders in the same chamber to obtain an average focal shift ratio.

Alternatively, the focal shift ratio may be obtained by unzipping a DNA molecule of known sequence and using the resulting unzipping signature as a calibration [36] (Fig. 9A). Although the unzipping method yields a more accurate estimation of the focal shift concordant with the results predicted by the contour length of DNA in stretching experiments, it requires prior calibration of linear position sensitivity and trap stiffness, as well as prior determination of both ssDNA and dsDNA linear elastic parameters [40-42].

In this method, a double-stranded DNA is mechanically separated via mechanical separation of the DNA bases by stretching the two DNA strands axially (Fig. 9A). For details of the unzipping DNA template design, we refer readers to previous descriptions [43-52]. After unzipping, an estimated focal shift is used to convert the piezo position z_{piezo} to trap height h_{trap} and thus z_{DNA}. The resulting measured force-extension unzipping curve is then correlated with the expected theoretical unzipping curve (Fig. 9B) [42,43]. The focal shift ratio is taken as the ratio that gives the highest correlation.

The detailed steps of the unzipping method are listed below:

1. Make a sample chamber containing cylinders tethered to the surface via the unzipping DNA template in PBS buffer. Seal the chamber with high vacuum grease.
2. Set the laser power to 20 mW.
3. Center the DNA over the cylinder laterally by stretching along the *x* and *y* direction.
4. Find the surface.
5. Unzip the DNA along the *z* axis and record z_{cyl}, P, and z_{piezo}.
6. Convert z_{cyl} and P to force F.
7. Convert z_{cyl}, z_{piezo}, and z_{p0} to z_{DNA} using an estimated f_s.
8. Calculate the theoretical force-extension curve.
9. Cross-correlate the measured force-extension curve with the theoretical force-extension curve.
10. Vary f_s to find the optimal correlation.

3.3.4 Calibrate Axial Position Detector and Axial Trap Stiffness

To determine the axial displacement sensitivity $S_z = \frac{-\Delta\zeta}{z_{\mathrm{cyl}}}$, we vertically stick a cylinder to the surface of a coverslip, and then move the trap axially through this stuck cylinder to measure the resulting $\Delta\zeta$ at different trap heights (Fig. 10A top panel). Because the cylinder is stuck, $h_{\mathrm{trap}} \equiv z_{\mathrm{cyl}}$, thus we can obtain the relationship between $\Delta\zeta$ and z_{cyl}. This calibration of the axial displacement sensitivity in an AOT is similar to that for a conventional axial optical trap [36].

1. Resuspend cylinders in Tris-HCl buffer, pH 8.0, (with 50 mM NaCl, 10 mM $MgCl_2$, and 0.1 mg/mL β-casein) by vigorous sonication for 1 minute. The Mg^{2+} ions in the buffer screen the surface charges of the cylinders, making it easier for the cylinders to stick to the sample chamber surface. Flow the cylinders into a sample chamber and seal the chamber with high vacuum grease.
2. Set the trapping laser power to 20 mW. Catch a cylinder using the optical trap and press the cylinder against the coverslip surface until ζ reaches a maximum value. At this position, the pressing force reaches the maximum value as well. Afterwards, set the laser power to a high value (350 mW) and wait for 10 seconds. This step is used to firmly stick the cylinder vertically to the surface. Set the laser power back to 20 mW and move the trap axially while recording $\Delta\zeta$ vs h_{trap}.
3. Repeat the step above on multiple cylinders in the same chamber.
4. Plot $\Delta\zeta$ vs h_{trap} from different cylinders (Fig. 10A, bottom panel). For the plot from each cylinder, perform a linear fit to the linear range close to $\Delta\zeta = 0$ to obtain a slope. S_z is the average value of the absolute slopes from different cylinders.

Once the axial displacement sensitivity S_z is calibrated, the axial trap stiffness k_z can be determined using the axial Brownian motion of the cylinder. Because the Brownian motion amplitude of a trapped cylinder is small, the potential energy E_z of a trapped cylinder is a quadratic function with respect to z_{cyl}, $E_z = k_z\langle {z_{\mathrm{cyl}}}^2\rangle/2$, where k_z is the axial trap stiffness. According to the equipartition theorem, the potential energy along this axis should be half of the thermal energy kT,

$$\frac{1}{2}k_z\langle {z_{\mathrm{cyl}}}^2\rangle = \frac{1}{2}kT, \qquad \text{Eq.7}$$

where k is Boltzmann's constant and T is the absolute temperature. In principle, by directly measuring the variance of the Brownian motion $\langle {z_{\mathrm{bead}}}^2\rangle$, we can obtain the trap stiffness. In practice, the Brownian motion measurement usually contains low-frequency noise due to drift in the detected signal, which tends to lead to an overestimation of the variance and under-estimation of k_z. Therefore, instead, we convert time-domain data into frequency domain data and use the power spectral density to more accurately determine the variance.

According to the Parseval theorem, the Brownian motion variance $\langle {z_{\mathrm{cyl}}}^2\rangle$ is equal to the power spectrum density (PSD) $\left|\tilde{\mathrm{z}}_{\mathrm{cyl}}(f)\right|^2$ integrated from negative infinity to positive infinity,

$$\langle {z_{\mathrm{cyl}}}^2\rangle = \int_{-\infty}^{+\infty}\left|\tilde{\mathrm{z}}_{\mathrm{cyl}}(f)\right|^2 \mathrm{d}f. \qquad \text{Eq.8}$$

For a cylinder trapped in a harmonic potential, $\left|\tilde{\mathrm{z}}_{\mathrm{cyl}}(f)\right|^2$ may be determined analytically. The Langevin equation of the particle motion can be written as

$$z_{\mathrm{cyl}}(t) + \beta\dot{z}_{\mathrm{cyl}}(t) = \Gamma(t), \qquad \text{Eq.9}$$

where β is the damping coefficient and $\Gamma(t)$ is the stochastic force which has a Gaussian white noise spectrum. Fourier transformation of the equation is

$$\tilde{z}_{\mathrm{cyl}}(f) = \frac{\tilde{\Gamma}(f)}{k_z + 2\pi f i\beta}. \qquad \text{Eq.10}$$

Hence, the power spectrum density has the form

$$\left|\tilde{z}_{\mathrm{cyl}}\right|^2 = \frac{A^2}{f_0^2 + f^2}, \qquad \text{Eq.11}$$

where $f_0 = \frac{k_z}{2\pi\beta}$ is the corner frequency, and $A^2 = \frac{\left|\tilde{\Gamma}\right|^2}{(2\pi\beta)^2}$. The Fourier transformation of the Gaussian white noise is a constant, so A is a constant.

To determine axial trap stiffness, we first obtain A and f_0 by fitting the measured PSD and use the resulting $\left|\tilde{z}_{\mathrm{cyl}}\right|^2$ to find the Brownian motion variance:

$$\langle {z_{\mathrm{cyl}}}^2\rangle = \int_{-\infty}^{\infty}\frac{A^2}{{f_0}^2 + f^2}\,df = \frac{\pi A^2}{f_0}. \qquad \text{Eq.12}$$

The stiffness is then written as follows

$$k_{\mathrm{z}} = \frac{kT}{\langle {z_{\mathrm{cyl}}}^2\rangle} = \frac{kTf_0}{\pi A^2}. \qquad \text{Eq.13}$$

Finally, the force exerted on the cylinder can be calculated by

$$F = k_z \cdot (-\Delta\zeta / S_z). \quad \text{Eq.14}$$

The detailed steps to determine the axial trap stiffness are listed below:

1. Construct a sample chamber containing cylinders re-suspended in the PBS buffer. Seal the chamber with high vacuum grease.
2. Set the laser power to 10 mW. Set the analog low-pass filter of the axial displacement signal to 5 KHz.
3. Trap a cylinder. Set the trap height to 1000 nm. Set the polarization angle to 0° (see later sections on how to specify the cylinder rotation angle). Record the axial displacement signal at a sampling rate of 10 kHz, following the Nyquist sampling theorem for minimizing aliasing, for a specific period, e.g., 10 s.
4. Fast Fourier-transform the measured $z_{\mathrm{cyl}}(t)$ to get its PSD. The resulting PSD spans a frequency range of 0 – 5 kHz.
5. Fit the PSD to obtain A and f_0 (Fig. 10B, top panel). To minimize contributions from break-through aliasing from the low-pass filtering and broad-spectrum electronic noise, we typically fit the data up to 1.5 kHz.
6. Calculate the axial trap stiffness at this laser power using Eq. 13.
7. Repeat the measurement at eight different polarization angles from 0° to 315°. Verify that the trap stiffness should be polarization-angle independent. Use the average value as the axial trap stiffness.
8. Repeat the measurement at different laser powers. Because the trap stiffness is proportional to the input laser power, the slope of the k_z versus laser power relation provides the trap stiffness per unit laser power (Fig. 10B, bottom panel).
9. Repeat the measurement on 20 different cylinders in the same chamber. Use the average value as the axial trap stiffness.

3.3.4 Force and its Trap Height Dependence

The axial displacement signal baseline ζ_0 corresponds to the force baseline $F = 0$. However, due to the spherical aberration of the trap in solution, ζ_0 increases with an increase

in the trap height h_{trap} (Fig. 8B). For a small trap height (< 1 μm), this effect may be negligible, but for a large trap height, which is necessary for working with longer DNA templates, this baseline must be properly removed in order to precisely determine the axial force. To characterize this baseline, we trapped an untethered cylinder and obtain the baseline signal ζ_0 vs trap height, and we found that this baseline appears to be linearly dependence on the trap height. In an experiment involving a DNA-tethered cylinder, this baseline is then removed from the measured ζ: $\Delta\zeta(h_{\mathrm{trap}}) = \zeta(h_{\mathrm{trap}}) - \zeta_0(h_{\mathrm{trap}})$.

3.4 Input Polarization Control and Characterization

In an AOT, rapid and flexible control of the polarization of the trapping laser beam input to the objective is essential, not only for rotating the trapped cylinder, but also for calibrating the cylinder's angular properties. In addition, any deviation of the polarization from the linear state must also be characterized to differentiate between polarization change introduced by a trapped cylinder from that in the input laser beam. Below, we describe methods to meet these goals.

3.4.1 Polarization State Control

We control the polarization of the trapping beam input to the objective via the "Input polarization rotator" [20]. At the rotator, the trapping laser beam is split into two beams of orthogonal polarizations (P and S), which then pass through AOM (P) and AOM (S), respectively (see Note 3). The two AOMs are driven by a dual channel computer-controlled digital RF frequency synthesizer with a center frequency of ~40 MHz. The AOMs are aligned to maximize the first-order diffracted beam with all other orders blocked. The amplitude and phase of each RF driver are rapidly and precisely controlled by a computer and determine the intensity and phase of the first-order diffracted beam, respectively. The two AOMs are tuned so that their first-order diffracted beams have the same intensity. After passing through the two AOMs, the beams are then recombined into two co-linear, overlapping beams (see Note 4). At this stage, the polarization state of the recombined beam is elliptically polarized. After passing through a

λ/4 located right before the objective, the two beams are then allowed to interfere, creating a linearly polarized beam (Fig. 11).

Thus, in this design, AOM (P) and AOM (S) generate the right (R) and left (L) circular components of the linearly polarized trapping laser. The change in the polarization angle $\Delta\Theta$ is specified by the phase difference $\Delta\varphi = \varphi_{\mathrm{P}} - \varphi_{\mathrm{S}}$ introduced by the AOMs: $\Delta\Theta = \frac{\Delta\varphi}{2}$ (Fig. 11). Using this method, the polarization angle can be specified at an arbitrary rate up to hundreds of kilohertz simply by modulating this phase difference of the two AOMs.

3.4.2 Detection of the Polarization State of the Laser Trap

Although a change in the laser polarization angle Θ is specified by the two AOMs, the absolute polarization angle needs to be established in real time. Thus, we have implemented an "input polarization angle detector" [20,39] (Fig. 2). A small sample of the beam (~1%) is reflected off the main optical path by a beam tap to monitor the input trapping beam polarization state. At the "input polarization angle detector", the light is split to two identical beams by a 50/50 cube. One of the beams is then decomposed along the horizontal direction and projected onto photodetector A (voltage readout V_A). For the other beam, its polarization direction is mirrored by a half wave plate at 22.5° first, then decomposed along the horizontal direction and projected onto photodetector B (voltage readout V_B) (Fig. 2). The polarization angle (Θ) is related to the detector signals (V_A and V_B) via the following relations:

$$V_{\mathrm{A}} = \sqrt{V_{\mathrm{A}}^2 + V_{\mathrm{B}}^2} \cdot \frac{\sin(2\Theta)+1}{2} \quad \text{and} \qquad \text{Eq. 15}$$

$$V_{\mathrm{B}} = \sqrt{V_{\mathrm{A}}^2 + V_{\mathrm{B}}^2} \cdot \frac{\cos(2\Theta)+1}{2}. \qquad \text{Eq. 16}$$

Since V_A and V_B contain measurement noise, we determine the angle Θ by minimizing the sum of squared difference (*SSD*) using Levenberg-Marquardt method:

$$SSD = \left[\frac{2V_{\mathrm{A}}}{\sqrt{V_{\mathrm{A}}^2+V_{\mathrm{B}}^2}} - 1 - \sin(2\Theta)\right]^2 + \left[\frac{2V_{\mathrm{B}}}{\sqrt{V_{\mathrm{A}}^2+V_{\mathrm{B}}^2}} - 1 - \cos(2\Theta)\right]^2. \qquad \text{Eq. 17}$$

In this method, the polarization angle from a previous time point can be used as an initial guess for the minimization process of the current time point to increase the computational speed.

In addition, in principle, the above design should result in a linearly polarized beam. In practice, a small degree of ellipticity may be introduced by various pieces of the optical components. This residual ellipticity, if uncharacterized, will result in uncertainties in the torque measurements. Thus, we have implemented the "input polarization ellipticity detector" that monitors this residual ellipticity in real time using the beam after the beam sampler (Fig. 2). At this detector, the beam is decomposed into P and S components, which also correspond to R- and L-circular components of the laser beam, respectively. Their powers are recorded by two photodetectors (P detector and S detector) (Fig. 2). For a linearly polarized trapping beam, the measured values of two photodetectors are initially tuned to be equal by modulating AOM P and AOM S, and any subsequent deviation from this equality indicates input beam ellipticity which will be removed from the final torque measurement. We also use the sum of these two detectors as a measure of the total trapping laser power.

3.5 Torque Generation and Detection Principle

In an AOT, the trapping cylinder is made of quartz, which has an anisotropic electric susceptibility $\overleftrightarrow{\chi}$: χ_{e} along the extraordinary axis is greater than χ_{o} along the ordinary axes, such that the extraordinary axis of the crystal is more easily polarized than the ordinary axes. Thus, the cylinder tends to align its extraordinary axis in the direction of the laser polarization, and if the extraordinary axis is not aligned with the laser polarization, an optical torque will be exerted on the cylinder [20].

This may be understood by examining the induced polarization $\vec{P}$ when the cylinder is subjected to an external electric field $\vec{E}$:

$$\vec{P} = \chi_{\mathrm{e}} E_{\mathrm{x}} \hat{x} + \chi_{\mathrm{o}} E_{\mathrm{y}} \hat{y}, \qquad \text{Eq. 18}$$

where $\hat{x}$ and $\hat{y}$ are unit vectors along the principal axes of the quartz crystal. Because $\chi_{\mathrm{e}} > \chi_{\mathrm{o}}$ for quartz, $\vec{P}$ and $\vec{E}$ are generally not in the same direction, except when $\vec{E}$ is aligned with one the principal axes. If $\vec{E}$ makes an angle θ with the extraordinary axis, the restoring torque on the cylinder is:

$$\vec{\tau} = \int d^3\vec{r}\, \vec{P} \times \vec{E} = \hat{z}\frac{1}{2}(\chi_{\mathrm{e}} - \chi_{\mathrm{o}})\sin(2\theta) \int d^3\vec{r}\, E_0^2(\vec{r}) = \hat{z}\tau_0 \sin(2\theta), \qquad \text{Eq.19}$$

where $\hat{z}$ is the unit vector along the direction of light propagation, and τ_0 is the maximum magnitude of torque exerted on the cylinder.

In addition to exerting torque on a trapped quartz cylinder, the AOT also directly measures the optical torque. When an optical torque is exerted on the cylinder, the trapping laser, which initially carried zero net angular momentum (linearly polarized), leaves the cylinder carrying a net angular momentum (elliptically polarized). The torque acting on the cylinder is equal and opposite to the rate of change of the angular momentum of the trapping beam as the beam passes through the cylinder. Each photon in a right-handed (RH) or left-handed (LH) circularly polarized light (CPL) carries $-\hbar$ or $+\hbar$ spin angular momentum, respectively. Thus, the torque exerted on the cylinder causes an imbalance of the power of LH and RH circular components (P_{L} and P_{R}) in the transmitted beam. Since each photon carries $\hbar\omega_0$ energy with ω_0 being the angular frequency of the laser, the optical torque is therefore:

$$\tau = (P_{\mathrm{R}} - P_{\mathrm{L}})/\omega_0, \qquad \text{Eq. 20}$$

where P_{R} and P_{L} are the powers of the RH CPL and LH CPL, respectively.

In an AOT, this optical torque is measured via the "torque detector", at which the transmitted light is decomposed into the left- and right-handed circular components and detected by the R photodetector (Voltage V_{R}) and the L photodetector (Voltage V_{L}), respectively (Fig. 2).

3.6 Torque Detector Calibration

In principle, torque may be obtained using Eq. 20. In practice, due to photon losses in the optical system, the R and L photodetectors cannot capture all of the transmitted beam. Thus, the torque detector signal $V_\tau = V_{\mathrm{R}} - V_{\mathrm{L}}$ needs to be calibrated to determine the pre-factor for conversion to $P_\tau = P_{\mathrm{R}} - P_{\mathrm{L}}$. This calibration procedure includes two steps [20]: 1) torque sensitivity calibration that converts the torque detector signal V_τ into θ, the deviation of the extraordinary axis of the cylinder from the trap polarization, and 2) angular trap stiffness calibration that converts θ to torque τ.

3.6.1 Torque Detector Sensitivity Calibration

The first step in the torque detector calibration is to relate V_τ to θ. Based on Eq. 19 and Eq. 20,

$$V_\tau = V_{\tau 0}\sin(2\theta), \qquad \text{Eq. 21}$$

where $V_{\tau 0}$ is the maximum value of the torque signal. Because V_τ is dependent on the laser power and force, to generalize Eq. 21, we normalize V_τ by the total power at the detector ($V_\mathrm{R} + V_\mathrm{L}$): $V_\tau' = \frac{V_\mathrm{R} - V_\mathrm{L}}{V_\mathrm{R} + V_\mathrm{L}}$:

$$V_\tau' = V_{\tau 0}'\sin(2\theta). \qquad \text{Eq. 22}$$

To determine $V_{\tau 0}{}'$, we rotate the laser polarization at such a rapid rate that the cylinder cannot keep up due to the viscous drag on the cylinder. Therefore, the polarization vector effectively scans a quasi-stationary cylinder. The detailed steps to determine $V_{\tau 0}{}'$ are listed below:

1. Construct a sample chamber containing cylinders re-suspended in PBS buffer. Seal the chamber with high vacuum grease.
2. Set the laser power to 10 mW. Trap a cylinder, and then move the cylinder to a trap height of 1000 nm.
3. Spin the polarization angle at 250 turns/s (Fig. 13A). Record the torque detector signal $V_\tau = V_\mathrm{R} - V_\mathrm{L}$ for 5 s at a sampling rate of 10 kHz (Fig. 13B). Fit the data with a sinusoidal function to obtain $V_{\tau 0}$, and find $V_{\tau 0}{}'$.
4. Repeat the measurements from steps 2-3 on 20 different cylinders in the same chamber.

Once $V_{\tau 0}{}'$ is determined, θ may then be found via the normalized torque signal $V_\tau{}'$ according to Eq. 22:

$$\theta = \sin^{-1}(V_\tau{}'/V_{\tau 0}{}')\,/2. \qquad \text{Eq. 23}$$

Under the limit where the angular displacement θ is small,

$$\theta \approx \frac{V_{\tau}{}'}{2V_{\tau 0}{}'} = \frac{V_{\tau}{}'}{S_\theta}. \qquad \text{Eq. 24}$$

We refer to S_θ as the angular sensitivity of the torque detector.

3.6.2 Angular Trap Stiffness Calibration

After θ is measured via the normalized torque detector signal V_τ', V_τ' can then be converted to torque τ as long as the angular trap stiffness k_θ is calibrated. We calibrate k_θ using the angular Brownian motion of the cylinder $\theta(t)$, akin to the method used for the axial trap stiffness calibration. For small angular fluctuations, the angular trapping potential is effectively harmonic. According to the equipartition theorem,

$$\frac{1}{2}k_\theta\langle\theta^2\rangle = \frac{1}{2}kT, \qquad \text{Eq. 25}$$

where k_θ is the angular stiffness of the trap. The Brownian motion variance $\langle\theta^2\rangle$ can be obtained directly or more accurately via the integral of the power spectrum density of the angular motion $\left|\tilde{\theta}(f)\right|^2$,

$$\langle\theta^2\rangle = \int_{-\infty}^{+\infty}\left|\tilde{\theta}\right|^2 \mathrm{d}f. \qquad \text{Eq. 26}$$

By fitting the power spectrum with a Lorentzian function $\left|\tilde{\theta}\right|^2 = A^2/(f_0^2 + f^2)$, we can obtain A and the corner frequency f_0 and thus obtain the angular trap stiffness by:

$$k_\theta = \frac{kTf_0}{\pi A^2}. \qquad \text{Eq. 27}$$

The torque can be calculated by

$$\tau = k_\theta\theta = \frac{k_\theta}{S_\theta}V_\tau'. \qquad \text{Eq. 28}$$

The detailed steps for angular stiffness calibration are like that for the calibration of the axial stiffness and are listed below:

1. Construct a sample chamber containing cylinders re-suspended in PBS buffer. Seal the chamber with high vacuum grease.
2. Set the laser power to 10 mW. Set the analog low-pass filter of the axial displacement signal to 5 kHz.
3. Trap a cylinder. Set the trap height to 1000 nm and the polarization angle Θ to 0°.
4. Record $\theta(t)$ at sampling rate of 10 kHz, following the Nyquist sampling theorem for minimizing aliasing, for 10 s.
5. Fast Fourier-transform $\theta(t)$ to get $\left|\tilde{\theta}\right|^2$.

6. Fit $\left|\tilde{\theta}\right|^2$ up to 1 kHz to obtain A and f_0. Obtain k_θ using Eq. 27. (Fig. 13B upper panel)
7. Repeat the measurement at seven additional angles from 45° to 315°. Use the average value of k_θ from the eight angles as the angular stiffness.
8. Repeat the measurement at different laser powers. Because the trap stiffness is proportional to the laser power, linearly fit the data k_θ versus laser power to obtain the angular trap stiffness per unit laser power (Fig. 13B lower panel).
9. Repeat the measurement on 20 different cylinders. Use the average value as the angular stiffness.

3.7 The Constant-Extension Method and Its Applications

In this section, we discuss our newly developed constant-extension method that enables the determination, via direct torque measurements, of the twist persistence length of extended DNA under very low forces, and the twist persistence length of a plectoneme [26]. This method expands the capabilities of the AOT and allows an increased understanding of DNA torsional parameters.

The torsional properties of the B-form of DNA are characterized by two parameters[53]: effective twist persistence length C_{eff} of extended DNA and twist persistence length P of plectonemic DNA. Both C_{eff} and P measure how much twist is introduced when turns are added to DNA and thus reflect the energetic cost to supercoil DNA. For an extended DNA molecule much longer than its bending persistence length, C_{eff} is expected to be force-dependent[54-57]: $C_{\mathrm{eff}}(F)$, increasing with force and plateauing to the intrinsic twist persistence length C. On the other hand, the twist persistence length P should be independent of force [53]. A comprehensive description of the torsional properties of DNA requires determination of $C_{\mathrm{eff}}(F)$ and P.

Traditionally, DNA torsional properties were conducted under a constant force using an AOT [21,23,27,24,25,29]. For example, using an AOT, the force in the DNA is clamped by a feedback loop that modulates the coverslip height to maintain a constant force on the cylinder at a constant laser power. Fig. 14 shows the measured extension and torque versus turns added to DNA of 6.1 kb and 12.7 kb under a constant force of 0.5 pN [26]. The turns are converted to

super-helical density σ, defined as the number of turns added or removed relative to the total number of turns in a relaxed DNA. These traces show that prior to DNA buckling (as evidenced by a sudden decrease in extension and a transition to a torque plateau), DNA extension remains nearly constant, and the torque in DNA increases with turns. The slope of the torque versus σ relation before buckling is used for conversion to the twist persistence length C_{eff} at the given force [23,29,26]. As expected, because of the scale invariance of DNA elastic properties, the torque versus σ for the templates are essentially identical. These measurements also demonstrate that the AOT can make accurate torsional measurements of long DNA molecules. Fig. 15A shows the measured extension and torque versus turns added to DNA of 12.7 kb under different forces. These measurements can be used to obtain C_{eff} versus F.

Although the constant-force method is effective at measuring C_{eff} when $F \geq 0.2\ pN$, measurements at much smaller forces are challenging as the measured force may contain an unknown offset, which is relatively small for large forces but significant for forces approaching zero. To overcome this limitation, we have developed the constant-extension method to determine C_{eff} at low force [26]. In this method, we take advantage of the AOT's ability to accurately determine the absolute DNA extension [39] and the established force-extension relation for DNA under no torsion [58,59] to identify the force offset at zero turns and remove it for all measured forces at non-zero turns. We have implemented the constant-extension method by modulation of the coverslip height to maintain a constant distance between the cylinder and coverslip [26] . As turns are introduced by the AOT at a specified DNA extension, the resulting force and torque are directly measured, and the force is corrected for the small force offset.

Fig. 15B shows an application of the constant-extension method using the 12.7 kb DNA. When turns are added, the force increases only slightly between -10 and +10 turns. However, the torque increased nearly linearly in this range, which corresponds to a range prior to DNA buckling [53,60]. Thus, the twist persistence length C_{eff} at a specific force is determined using the slope of the torque signal over this range. The four extensions then lead to measured C_{eff} at four different forces. Note that the smallest force obtained is ~0.02 pN (or 20 fN), an order of

magnitude smaller than attainable via the constant-force method. At this force, the measured $C_{\mathrm{eff}} = 22 \pm 3$ nm, which is about 20% of the intrinsic twist persistence length $C = 109.3$ nm.

Below, we list the steps for torsional property measurement of a 12.7 kb DNA template by the constant-extension method:

1. Prepare a chamber containing 12.7 kb DNA molecules, each of which is torsionally anchored to the surface of the coverslip at one end and to the bottom of cylinder at the other end.
2. Set the laser power to 20 mW.
3. Center the trap over a tethered cylinder.
4. Find the surface: $h_{\mathrm{trap}} = 0$.
5. Stretch the DNA such that $z_{\mathrm{DNA}} = 500$ nm. Activate the extension clamp to maintain $z_{\mathrm{DNA}} = 500$ nm. Measure the force offset.
6. Twist the DNA to -10 turns and then to +10 turns at 1 turns/s. If the tether is torsionally constrained, force will increase with an increase in turns added. If not, go back to step 3. Force and torque data are analog filtered to 5 kHz, digitized at 10 kHz, and further filtered to 5 Hz.
7. Repeat steps 1-6 for multiple different DNA molecules in the same chamber to obtain averaged measurements.

The constant-force method is also ideally suited for measurement of the torsional stiffness of a plectonemic DNA. This experiment can be done in a similar fashion as those of Fig. 15B by introducing a large number of turns to ensure that DNA is predominately plectonemic. Fig. 15C shows an example of such a measurement under 500 nm extension, which is much smaller than the DNA contour length of 4300 nm. This extension is chosen to minimize any contributions from the extended DNA region to the measurements and to limit potential interactions of DNA with the surfaces of the cylinder and coverslip that could exist at smaller extensions. A linear fit to the torque versus turn data yields $P = 24$ nm.

4 Notes

1. The nanofabrication protocol outlined here can readily be modified to produce somewhat larger cylinders (e.g., cylinders of 1 μm diameter and 2 μm height) if greater torques and forces are desired.
2. In the first step of the cylinder functionalization when the fresh-cut cylinder is suspended in PBS, the cylinders tend to stick to the side wall of the plastic centrifuge tubes, making it hard to compactly pellet the cylinders. To solve this issue, we sonicate the tube transiently in the middle of centrifuging to re-suspend those cylinders attached to the side wall. This step may need to be repeated several times before all cylinders are pelleted. The cylinders will become less sticky in the rest of the steps.
3. Leakage of light from PBSC1 will contaminate the other component with light of the incorrect phase, therefore we used two polarizers (P2 and P3) after the AOMs to further purify the polarizations.
4. It is important to align the P and S beam so they are collinear, otherwise the P and S beams will form separate traps at the specimen plane. The misaligned P and S beams will cause severe issues in both the data acquisition and the data analysis.

Acknowledgements

We thank Drs. R.M. Fulbright and S.L. Moore for commenting on this chapter. M.D.W. is a Howard Hughes Medical Institute Investigator. This work was supported by the National Institutes of Health grant R01GM136894 to M.D.W. The quartz cylinder fabrication was performed at the Cornell NanoScale Science & Technology Facility (CNF), a member of the National Nanotechnology Coordinated Infrastructure (NNCI), which is supported by NSF (NNCI-1542081).

Figure Captions

Figure 1. Experimental configuration to study torsional properties of DNA using an AOT. The AOT has enabled direct control and detection of torque and rotation in individual biomolecules. The trapping particle of an AOT is typically a nanofabricated quartz cylinder. Shown is an example of using an AOT to study torsional properties of DNA. Here, one end of the DNA is torsionally anchored to the bottom surface of the cylinder, and the other end is torsionally anchored to the coverslip surface of a sample chamber. As DNA is supercoiled via rotation of the cylinder, the torque in the DNA as well as the force in the DNA and DNA extension are simultaneously measured. Adapted from reference [29] with permission from Cell Press.

Figure 2. Schematic of the AOT. An input laser beam is collimated by a pair of lenses (L1 and L2) and is linearly polarized to 45° by a combination of a λ/2 plate and polarizer P1. The beam then passes through an 'input polarization rotator'. At the rotator, the beam is split equally at a polarization beam splitting cube (PBSC) into two orthogonally polarized beams (P beam and S beam). Each beam is sent through one AOM (AOM P or S), which can modulate the phase and amplitude of the beam. The two beams are recombined at another PBSC, resulting in two overlapping and co-linear beams with their phase difference $\varphi(t)$ controlled by the two AOMs. This phase difference eventually translates into a rotation of the polarization $\Delta\Theta = \Delta\varphi/2$ by a λ/4 plate located immediately before the objective. Prior to the objective, a small fraction of the recombined beam is sampled by a beam tap, directed to a 50/50 beam splitter, and split to two beams. One beam is sent to the 'input polarization ellipticity detector' that measures the ellipticity and power of the laser beam via photodetectors P and S, while the other beam is sent to the 'input polarization angle detector' that measures the polarization angle via photodetectors A and B. After the light interacts with a trapped cylinder in the specimen plane, the transmitted laser becomes elliptically polarized, and the optical torque is measured by the 'torque detector' via photodetectors R and L. The force on the cylinder is measured by a quadrant photodiode (QPD).

Notation: polarization beam splitter cube (PBSC), acousto-optic modulator (AOM), polarizer (P), photodetectors (denoted as A, B, P, S, R, and L). lens (L), mirror (M); dichroic mirror (DM), infrared KG glass filter (KG), quadrant photodiode (QPD).

Figure 3. Nanofabrication of quartz cylinders.

(A) Schematic outline of the nanofabrication protocol.

(B–E) SEM images of nanofabricated cylinders. B and C show nanofabricated cylindrical posts on the wafer. The cylinders are 1.1 μm high and 0.53 μm in diameter. D shows quartz substrate after removal of a portion of the posts. E shows a single quartz cylinder after mechanical removal. Scale bars, 5 μm in B and 1 μm in C–E.

Adapted from reference [21] with permission.

Figure 4. A cartoon of a DNA template for torsional measurements. The DNA sequence of interest is flanked with multiple-biotin adaptor at one end and multi-digoxigenin adaptor at the other end.

Figure 5. Chamber preparation.

(A) A cartoon demonstrating how to prepare a sample chamber. The sample chamber is sandwiched between a glass coverslip and a glass slide. First, place two thin strips of double-sided sticky tape near the edge of the coverslip. Then, lay two lines of high vacuum grease using a syringe so that these two grease lines, spaced by about 6 mm, are inside the two tape strips. A glass slide is then placed on top of the coverslip to form a sandwich structure. The sample chamber is formed between the two grease lines.

(B) A photo of a sample chamber.

Figure 6. Definition of the focal shift. A cartoon to illustrate the origin of the focal shift.

(A) The coverslip of sample chamber is raised until it just touches the bottom surface of the cylinder, and this position is defined as $h_{\mathrm{trap}} = 0$.

(B) When the *z* piezo moves the coverslip down by z_{piezo}, the trap center also moves downwards because of the index of refraction mismatch at the water-glass interface, so $h_{\mathrm{trap}} < z_{\mathrm{piezo}}$. The initial trap position and final trap position are indicated by the intersections of dashed lines and solid lines, respectively. The ratio $\Delta h_{\mathrm{trap}}/\Delta z_{\mathrm{piezo}}$ is defined as the focal shift ratio f_{s}.

(C) When a DNA molecule is stretched axially, the attached cylinder will axially move downward from the equilibrium position (the position of a cylinder under no external force). The axial displacement is defined as z_{cyl}, and the DNA extension can be calculated from h_{trap} and z_{cyl}.

Figure 7. Determination of the surface position of a cylinder.

(A) A cartoon representation of the method.

(B) A representative plot of the measured ζ vs *z* piezo position z_{piezo}. By fitting to the experimental data (black solid line) with a two-piece function (Eq. 4) composing a parabola (green solid line) and a horizontal line (red solid line), the surface can be determined by the intersection point. Increasing z_{piezo} moves the coverslip away from the trap center (see Fig. 6), with $z_{\mathrm{piezo}} = 0$ at the highest possible piezo position.

(C) A more accurate method to find the surface position. The plot shows the measured surface position as indicated by the focal-shift corrected piezo position as a function of the laser power. Due to the Brownian motion of the cylinder, the cylinder senses the surface before its equilibrium position reaches the surface. The data are fit using the Brownian motion amplitude $\sqrt{\langle z_{\mathrm{cyl}}^2 \rangle} = \sqrt{kT/k_z}$, where kT is the thermal energy, and k_z is the axial trap stiffness, but with an offset, which gives the actual position of the surface that can be approached at infinitely large power.

Figure 8. Focal shift calibration via Fabry-Pérot interference.

(A) A cartoon to illustrate the interference between direct-through beam (red) and the reflected beam (blue).

(B) A representative ζ vs ($z_{\mathrm{piezo}} - z_{\mathrm{p0}}$) plot for the focal shift measurement. The focal shift is determined by fitting the data (black solid line) with a damped sinusoidal function (red solid line) (Eq. 5).

Figure 9. Focal shift calibration via DNA unzipping.

(A) A cartoon to illustrate the configuration of a DNA unzipping experiment. A Y-structure DNA molecule composed of two short arms and a long trunk segment is stretched by the AOT at a constant velocity and a constant laser power. This leads to unzipping of the trunk segment, and the unzipping force provides an accurate measure of the trap position.

(B) Theoretical force-extension relationship (red solid line) and experimental data (black solid line).

Figure 10. Axial position detector and axial trap stiffness calibration.

(A) Axial position detector calibration experiment. The piezo moves upward and downward near the trap center of the stuck cylinder, and $\Delta\zeta$ vs h_{trap} is recorded. A linear fitting (black solid line) to the measured data (colored curves) near zero h_{trap} is used to determine the axial trap sensitivity.

(B) Axial trap stiffness calibration. The top plot shows the power spectral density (PSD) of the axial Brownian motion of an untethered cylinder trapped by 10 mW of laser. To determine the axial Brownian motion variance $\langle z_{\mathrm{cyl}}^2 \rangle$, the measured power spectral density (black) is fitted by a Lorentzian function (red solid line) and then the fitting function is integrated to obtain $\langle z_{\mathrm{cyl}}^2 \rangle$. $\langle z_{\mathrm{cyl}}^2 \rangle$ is then used to obtain the trap stiffness k_z. The bottom plot shows k_z versus laser power. The slope gives the axial stiffness per unit laser power.

Figure 11. Schematic explanation of the method of polarization rotation.

The first column indicates the phase difference $\Delta\varphi$ between P and S linearly polarized beams. The second column shows the combined field of these two polarizations of the same amplitude. The third column shows a snapshot of the polarization state after conversion by a λ/4 plate,

which converts P and S beams into right-handed and left-handed circularly polarized beams respectively. This leads to linearly polarized light with the direction of the polarization Θ determined by $\Delta\varphi$.

Figure 12. Torque generation and detection principles of the AOT. In an AOT, the trapped particle is a nanofabricated quartz cylinder that, when trapped, aligns its cylinder axis along the direction of light propagation. When the incoming laser beam is linearly polarized with the electric field $\vec{E}_{\text{in}}$, the quartz cylinder develops a polarization $\vec{P}$ depending on the electric susceptibility $\overleftrightarrow{\chi}$ of the cylinder, which is anisotropic (χ_{e} along the extraordinary axis is greater than χ_{o} along the ordinary axes for quartz). The cylinder is fabricated so that the extraordinary axis is perpendicular to the cylinder axis. If $\vec{E}_{\text{in}}$ is not along one of the principal axes of the cylinder, the cylinder will experience a torque τ to align its extraordinary axis with the polarization (see Eq. 19), while the transmitted beam $\vec{E}_{\text{out}}$ becomes elliptically polarized. The torque on the cylinder is detected via this change in the polarization state of the light.

Adapted and revised from reference [29] with permission.

Figure 13. Torque detector sensitivity and angular trap stiffness calibrations.

(A) Angular sensitivity calibration. An untethered cylinder is trapped, and the laser polarization angle is rotated at a rapid rate so that the cylinder is quasi-stationary. The measured $V_\tau{}'$ shows a sinusoidal pattern with a period of around half a turn.

(B) Angular trap stiffness calibration. Top shows the power spectral density of the Brownian angular motion of a cylinder trapped with 10 mW laser power (black solid line). To determine the Brownian motion variance $\langle\theta^2\rangle$, the power spectral density is fitted by a Lorentzian function (red solid line), and then the fitting function is integrated to obtain the $\langle\theta^2\rangle$. The bottom shows the measured angular trap stiffness as a function of laser power. The slope gives the angular stiffness per unit laser power.

Figure 14. Measured torque and extension of DNA molecules with different lengths. Extension (**A**) and torque (**B**) measurements for naked DNA molecules of 12.7 kbp (red) and 6.1 kbp

(black) in length are shown. The experiments were conducted under 0.5 pN of force. As twist was introduced to a DNA molecule, torque increased essentially linearly until the DNA buckled to form a plectoneme, after which the torque plateaued. Vertical dashed lines indicate buckling transitions. Because the torsional mechanics of DNA is scale invariant, torque versus superhelical density should be independent of DNA length. Indeed, the measurements verified this within measurement uncertainty. Experiments were carried out in a buffer containing 10 mM Tris-HCl pH 8.0, 50 mM NaCl, 50 mM KCl, 3 mM $MgCl_2$, 0.1 mM EDTA, 1 mM DTT, 0.5 mM TCEP, 1 mM ATP, and 1.5 mg/mL β-casein.

Adapted from reference [29] with permission.

Figure 15. Torque measurements by an AOT of an extended and plectonemic DNA using either the constant-force or the constant-extension method. In both methods, a DNA molecule was torsionally constrained between a coverslip surface and a nanofabricated quartz cylinder held in the AOT. Top panels of Fig. A, B and C are cartoon representations of experimental configurations in these experiments. The same buffer as that for Fig. 14 was used.

(A) Constant-force method to measure the torsional properties of an extended DNA molecule. As turns were introduced to DNA with the force in the DNA held constant, the DNA extension (middle) and torque (bottom) were simultaneously measured. The C_{eff} at 0.25 pN, 0.5 pN, 1 pN, 2 pN, and 5 pN are 68 nm, 80 nm, 92 nm, 95 nm and 101 nm, respectively.

(B) Constant-extension method to measure the torsional properties of an extended DNA molecule. As turns were introduced to DNA with the DNA extension held constant, the force (middle) and torque (bottom) on the DNA were simultaneously measured. Notably, the force on the DNA in constant-extension experiments can be much lower than the smallest attainable force in previous constant-force measurements. The C_{eff} at 500 nm (0.02 pN), 1000 nm (0.04 pN), 2000 nm (0.11 pN), and 2800 nm (0.24 pN) are 22 nm, 28 nm, 42 nm and 65 nm, respectively.

(C) Constant-extension method to measure the twist persistence length P of plectonemic DNA. Both force (middle) and torque (bottom) were simultaneously measured as a function of turns

(red curves). P was determined by the slope of a linear fit to the torque-turns relation (bottom panel, black line) between +24 turns and +190 turns. The linear fit yields P = 24 ± 0.3 nm.

Adapted from reference [26] with permission.

References

1. Liu LF, Wang JC (1987) Supercoiling of the DNA template during transcription. Proc Natl Acad Sci U S A 84 (20):7024-7027. doi:10.1073/pnas.84.20.7024

2. Watson JD, Crick FH (1953) The structure of DNA. Cold Spring Harb Symp Quant Biol 18:123-131. doi:10.1101/sqb.1953.018.01.020

3. Kouzine F, Liu J, Sanford S, Chung HJ, Levens D (2004) The dynamic response of upstream DNA to transcription-generated torsional stress. Nat Struct Mol Biol 11 (11):1092-1100. doi:nsmb848 [pii]

10.1038/nsmb848

4. Kouzine F, Sanford S, Elisha-Feil Z, Levens D (2008) The functional response of upstream DNA to dynamic supercoiling in vivo. Nat Struct Mol Biol 15 (2):146-154. doi:10.1038/nsmb.1372

nsmb.1372 [pii]

5. Ma J, Wang MD (2014) RNA polymerase is a powerful torsional motor. Cell Cycle 13 (3):337-338. doi:Doi 10.4161/Cc.27508

6. Ma J, Wang MD (2014) Interplay between DNA supercoiling and transcription elongation. Transcription 5. doi:28636 [pii]

7. Ma J, Wang MD (2016) DNA supercoiling during transcription. Biophysical Reviews 8 (1):75-87. doi:10.1007/s12551-016-0215-9

8. Kouzine F, Gupta A, Baranello L, Wojtowicz D, Ben-Aissa K, Liu J, Przytycka TM, Levens D (2013) Transcription-dependent dynamic supercoiling is a short-range genomic force. Nat Struct Mol Biol 20 (3):396-403. doi:10.1038/nsmb.2517

nsmb.2517 [pii]

9. Naughton C, Avlonitis N, Corless S, Prendergast JG, Mati IK, Eijk PP, Cockroft SL, Bradley M, Ylstra B, Gilbert N (2013) Transcription forms and remodels supercoiling domains unfolding large-scale chromatin structures. Nat Struct Mol Biol 20 (3):387-395. doi:10.1038/nsmb.2509

nsmb.2509 [pii]

10. Teves SS, Henikoff S (2014) Transcription-generated torsional stress destabilizes nucleosomes. Nat Struct Mol Biol 21 (1):88-94. doi:10.1038/nsmb.2723

nsmb.2723 [pii]

11. Svoboda K, Block SM (1994) Biological Applications of Optical Forces. Annual Review of Biophysics and Biomolecular Structure 23:247-285. doi:DOI 10.1146/annurev.bb.23.060194.001335

12. Bustamante CJ, Chemla YR, Liu S, Wang MD (2021) Optical tweezers in single-molecule biophysics. Nature Reviews Methods Primers 1 (1):25. doi:10.1038/s43586-021-00021-6

13. Wang MD (1999) Manipulation of single molecules in biology. Current Opinion in Biotechnology 10 (1):81-86. doi:Doi 10.1016/S0958-1669(99)80015-9

14. Yin H, Wang MD, Svoboda K, Landick R, Block SM, Gelles J (1995) Transcription against an applied force. Science 270 (5242):1653-1657

15. Wang MD, Schnitzer MJ, Yin H, Landick R, Gelles J, Block SM (1998) Force and velocity measured for single molecules of RNA polymerase. Science 282 (5390):902-907

16. Wang MD, Yin H, Landick R, Gelles J, Block SM (1997) Stretching DNA with optical tweezers. Biophys J 72 (3):1335-1346. doi:S0006-3495(97)78780-0 [pii]

10.1016/S0006-3495(97)78780-0

17. Brower-Toland BD, Smith CL, Yeh RC, Lis JT, Peterson CL, Wang MD (2002) Mechanical disruption of individual nucleosomes reveals a reversible multistage release of DNA. Proceedings of the National Academy of Sciences of the United States of America 99 (4):1960-1965. doi:DOI 10.1073/pnas.022638399

18. Hall MA, Shundrovsky A, Bai L, Fulbright RM, Lis JT, Wang MD (2009) High-resolution dynamic mapping of histone-DNA interactions in a nucleosome. Nature Structural & Molecular Biology 16 (2):124-129. doi:Doi 10.1038/Nsmb.1526

19. Johnson DS, Bai L, Smith BY, Patel SS, Wang MD (2007) Single-molecule studies reveal dynamics of DNA unwinding by the ring-shaped T7 helicase. Cell 129 (7):1299-1309. doi:DOI 10.1016/j.cell.2007.04.038

20. La Porta A, Wang MD (2004) Optical torque wrench: Angular trapping, rotation, and torque detection of quartz microparticles. Physical Review Letters 92 (19). doi:Artn 190801

Doi 10.1103/Physrevlett.92.190801

21. Deufel C, Forth S, Simmons CR, Dejgosha S, Wang MD (2007) Nanofabricated quartz cylinders for angular trapping: DNA supercoiling torque detection. Nature Methods 4 (3):223-225. doi:Doi 10.1038/Nmeth1013

22. Forth S, Sheinin MY, Inman J, Wang MD (2013) Torque measurement at the single-molecule level. Annu Rev Biophys 42:583-604. doi:10.1146/annurev-biophys-083012-130412

23. Forth S, Deufel C, Sheinin MY, Daniels B, Sethna JP, Wang MD (2008) Abrupt buckling transition observed during the plectoneme formation of individual DNA molecules. Physical Review Letters 100 (14). doi:Artn 148301

Doi 10.1103/Physrevlett.100.148301

24. Sheinin MY, Forth S, Marko JF, Wang MD (2011) Underwound DNA under Tension: Structure, Elasticity, and Sequence-Dependent Behaviors. Physical Review Letters 107 (10). doi:Artn 108102

Doi 10.1103/Physrevlett.107.108102

25. Sheinin MY, Wang MD (2009) Twist-stretch coupling and phase transition during DNA supercoiling. Physical Chemistry Chemical Physics 11 (24):4800-4803. doi:Doi 10.1039/B901646e

26. Gao X, Hong Y, Ye F, Inman JT, Wang MD (2021) Torsional Stiffness of Extended and Plectonemic DNA. Physical Review Letters 127 (2):028101. doi:10.1103/PhysRevLett.127.028101

27. Forth S, Deufel C, Patel SS, Wang MD (2011) Direct Measurements of Torque During Holliday Junction Migration. Biophysical Journal 101 (2):L5-L7. doi:DOI 10.1016/j.bpj.2011.05.066

28. Sheinin MY, Li M, Soltani M, Luger K, Wang MD (2013) Torque modulates nucleosome stability and facilitates H2A/H2B dimer loss. Nat Commun 4:2579. doi:10.1038/ncomms3579

ncomms3579 [pii]

29. Le TT, Gao X, Park SH, Lee J, Inman JT, Lee JH, Killian JL, Badman RP, Berger JM, Wang MD (2019) Synergistic Coordination of Chromatin Torsional Mechanics and Topoisomerase Activity. Cell 179 (3):619-631 e615. doi:S0092-8674(19)31115-8 [pii]

10.1016/j.cell.2019.09.034

30. Ma J, Bai L, Wang MD (2013) Transcription under torsion. Science 340 (6140):1580-1583. doi:10.1126/science.1235441

340/6140/1580 [pii]

31. Ma J, Tan C, Gao X, Fulbright RM, Jr., Roberts JW, Wang MD (2019) Transcription factor regulation of RNA polymerase's torque generation capacity. Proc Natl Acad Sci U S A 116 (7):2583-2588. doi:10.1073/pnas.1807031116

1807031116 [pii]

32. Inman J, Forth S, Wang MD (2010) Passive torque wrench and angular position detection using a single-beam optical trap. Opt Lett 35 (17):2949-2951

33. Nicholas MP, Rao L, Gennerich A (2014) Covalent Immobilization of Microtubules on Glass Surfaces for Molecular Motor Force Measurements and Other Single-Molecule Assays. Mitosis: Methods and Protocols 1136:137-169. doi:10.1007/978-1-4939-0329-0_9

34. Rohrbach A, Stelzer EHK (2002) Three-dimensional position detection of optically trapped dielectric particles. J Appl Phys 91 (8):5474-5488. doi:10.1063/1.1459748

35. Gittes F, Schmidt CF (1998) Interference model for back-focal-plane displacement detection in optical tweezers. Opt Lett 23 (1):7-9. doi:Doi 10.1364/Ol.23.000007

36. Deufel C, Wang MD (2006) Detection of forces and displacements along the axial direction in an optical trap. Biophysical Journal 90 (2):657-667. doi:DOI 10.1529/biophysj.105.065458

37. Dreyer JK, Berg-Sorensen K, Oddershede L (2004) Improved axial position detection in optical tweezers measurements. Appl Optics 43 (10):1991-1995. doi:Doi 10.1364/Ao.43.001991

38. Neuman KC, Abbondanzieri EA, Block SM (2005) Measurement of the effective focal shift in an optical trap. Opt Lett 30 (11):1318-1320. doi:Doi 10.1364/Ol.30.001318

39. Ma J, Tan C, Wang MD (2018) Single-Molecule Angular Optical Trapping for Studying Transcription Under Torsion. Methods Mol Biol 1805:301-332. doi:10.1007/978-1-4939-8556-2_16

40. Koch SJ, Wang MD (2003) Dynamic force spectroscopy of protein-DNA interactions by unzipping DNA. Physical Review Letters 91 (2). doi:Artn 028103

Doi 10.1103/Physrevlett.91.028103

41. Koch SJ, Shundrovsky A, Jantzen BC, Wang MD (2002) Probing protein-DNA interactions by unzipping a single DNA double helix. Biophysical Journal 83 (2):1098-1105

42. Shundrovsky A, Smith CL, Lis JT, Peterson CL, Wang MD (2006) Probing SWI/SNF remodeling of the nucleosome by unzipping single DNA molecules. Nature Structural & Molecular Biology 13 (6):549-554. doi:Doi 10.1038/Nsmb1102

43. Li M, Wang MD (2012) Unzipping Single DNA Molecules to Study Nucleosome Structure and Dynamics. Nucleosomes, Histones & Chromatin, Pt B 513:29-58. doi:Doi 10.1016/B978-0-12-391938-0.00002-1

44. Li M, Hada A, Sen P, Olufemi L, Hall MA, Smith BY, Forth S, McKnight JN, Patel A, Bowman GD, Bartholomew B, Wang MD (2015) Dynamic regulation of transcription factors by nucleosome remodeling. Elife 4. doi:10.7554/eLife.06249

45. Brennan LD, Forties RA, Patel SS, Wang MD (2016) DNA looping mediates nucleosome transfer. Nat Commun 7:13337. doi:10.1038/ncomms13337

ncomms13337 [pii]

46. Sun B, Johnson DS, Patel G, Smith BY, Pandey M, Patel SS, Wang MD (2011) ATP-induced helicase slippage reveals highly coordinated subunits. Nature 478 (7367):132-U148. doi:Doi 10.1038/Nature10409

47. Sun B, Pandey M, Inman JT, Yang Y, Kashlev M, Patel SS, Wang MD (2015) T7 replisome directly overcomes DNA damage. Nat Commun 6:10260. doi:10.1038/ncomms10260

ncomms10260 [pii]

48. Sun B, Singh A, Sultana S, Inman JT, Patel SS, Wang MD (2018) Helicase promotes replication re-initiation from an RNA transcript. Nat Commun 9 (1):2306. doi:10.1038/s41467-018-04702-x

10.1038/s41467-018-04702-x [pii]

49. Le TT, Yang Y, Tan C, Suhanovsky MM, Fulbright RM, Jr., Inman JT, Li M, Lee J, Perelman S, Roberts JW, Deaconescu AM, Wang MD (2018) Mfd Dynamically Regulates Transcription via a Release and Catch-Up Mechanism. Cell 172 (1-2):344-357 e315. doi:S0092-8674(17)31364-8 [pii]

10.1016/j.cell.2017.11.017

50. Inman JT, Smith BY, Hall MA, Forties RA, Jin J, Sethna JP, Wang MD (2014) DNA y structure: a versatile, multidimensional single molecule assay. Nano Lett 14 (11):6475-6480. doi:10.1021/nl503009d

51. Sun B, Wang MD (2017) Single-Molecule Optical-Trapping Techniques to Study Molecular Mechanisms of a Replisome. Methods Enzymol 582:55-84. doi:S0076-6879(16)30248-8 [pii]

10.1016/bs.mie.2016.08.001

52. Killian JL, Inman JT, Wang MD (2018) High-Performance Image-Based Measurements of Biological Forces and Interactions in a Dual Optical Trap. ACS Nano. doi:10.1021/acsnano.8b03679

53. Marko JF (2007) Torque and dynamics of linking number relaxation in stretched supercoiled DNA. Phys Rev E Stat Nonlin Soft Matter Phys 76 (2 Pt 1):021926. doi:10.1103/PhysRevE.76.021926

54. Moroz JD, Nelson P (1997) Torsional directed walks, entropic elasticity, and DNA twist stiffness. Proc Natl Acad Sci U S A 94 (26):14418-14422. doi:10.1073/pnas.94.26.14418

55. Moroz JD, Nelson P (1998) Entropic elasticity of twist-storing polymers. Macromolecules 31 (18):6333-6347. doi:Doi 10.1021/Ma971804a

56. Bouchiat C, Mezard M (1998) Elasticity model of a supercoiled DNA molecule. Physical Review Letters 80 (7):1556-1559. doi:DOI 10.1103/PhysRevLett.80.1556

57. Bouchiat C, Mezard M (2000) Elastic rod model of a supercoiled DNA molecule. European Physical Journal E 2 (4):377-402. doi:DOI 10.1007/s101890050020

58. Marko JF, Siggia ED (1995) Stretching DNA. Macromolecules 28 (26):8759-8770. doi:Doi 10.1021/Ma00130a008

59. Bouchiat C, Wang MD, Allemand JF, Strick T, Block SM, Croquette V (1999) Estimating the persistence length of a worm-like chain molecule from force-extension measurements. Biophysical Journal 76 (1):409-413

60. Marko JF, Siggia ED (1994) Fluctuations and Supercoiling of DNA. Science 265 (5171):506-508. doi:DOI 10.1126/science.8036491

Figure 1

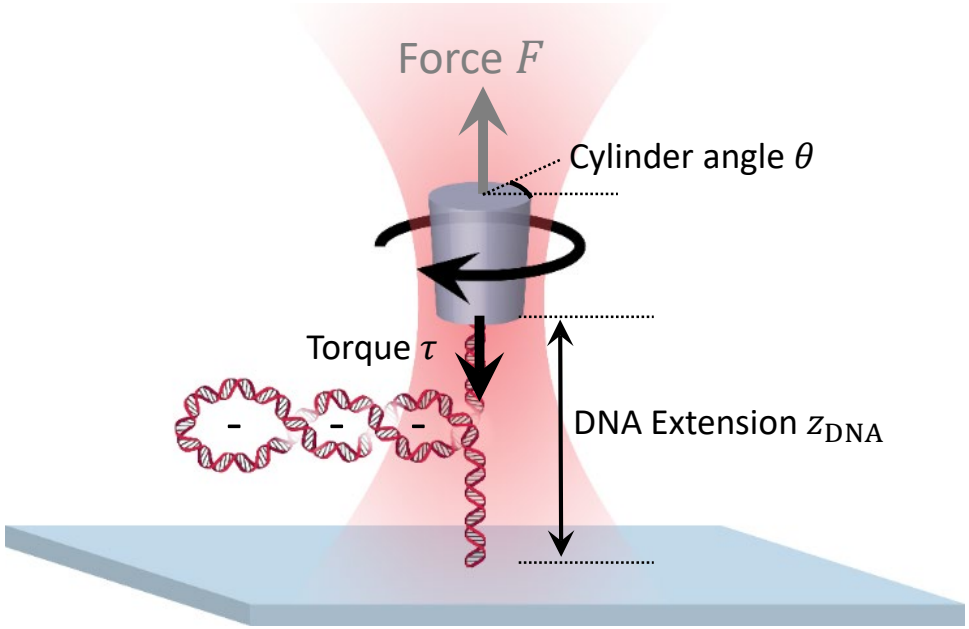
Force F
Cylinder angle θ
Torque τ
DNA Extension z_{DNA}

Figure 2

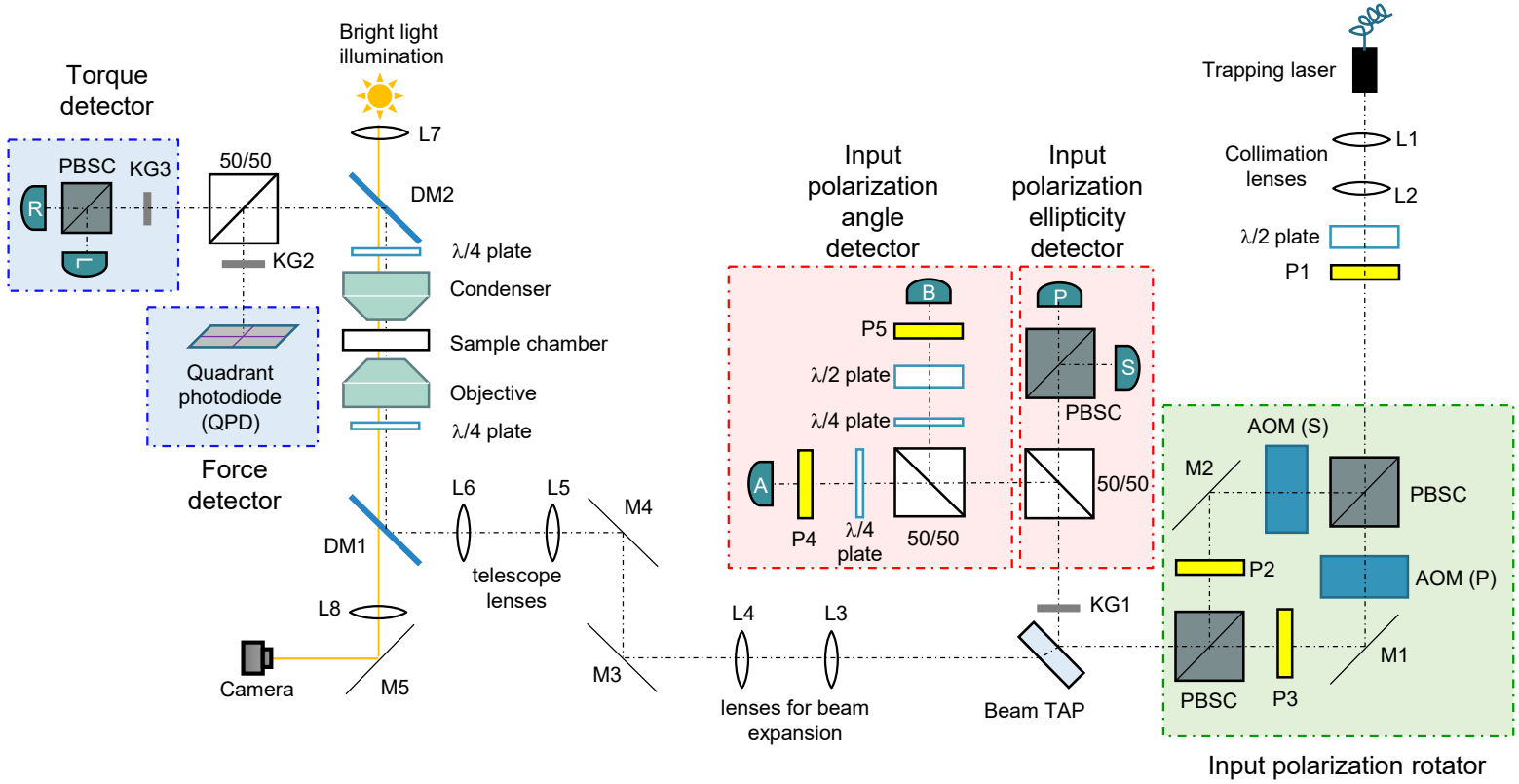
Torque detector
PBSC
KG3
R
50/50
KG2
Quadrant photodiode (QPD)
Force detector
Bright light illumination
L7
DM2
λ/4 plate
Condenser
Sample chamber
Objective
λ/4 plate
DM1
L6
L5
telescope lenses
M4
L8
Camera
M5
M3
L4
L3
lenses for beam expansion
Input polarization angle detector
B
P5
λ/2 plate
λ/4 plate
A
P4
λ/4 plate
50/50
Input polarization ellipticity detector
P
S
PBSC
50/50
KG1
Beam TAP
Trapping laser
Collimation lenses
L1
L2
λ/2 plate
P1
AOM (S)
M2
PBSC
P2
AOM (P)
PBSC
P3
M1
Input polarization rotator

Figure 3

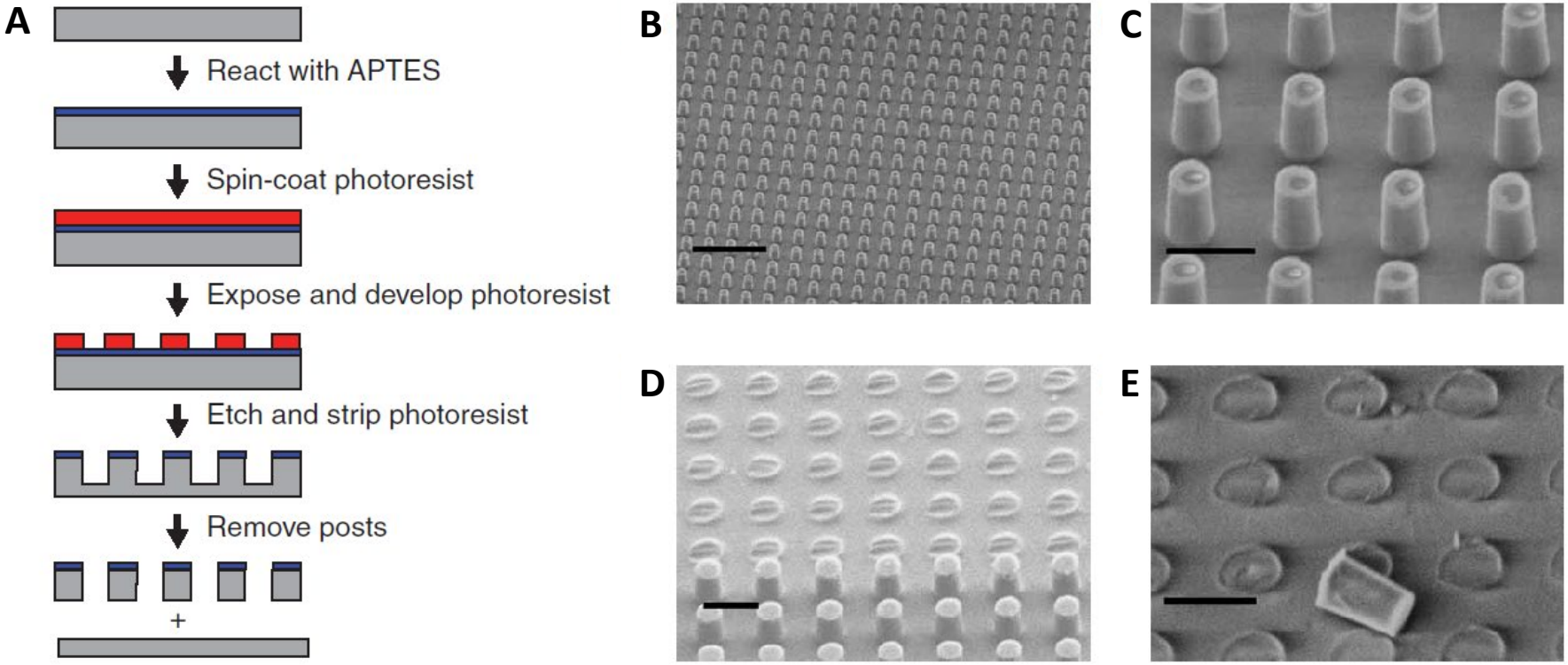
A
React with APTES
Spin-coat photoresist
Expose and develop photoresist
Etch and strip photoresist
Remove posts
+
B
C
D
E

Figure 4

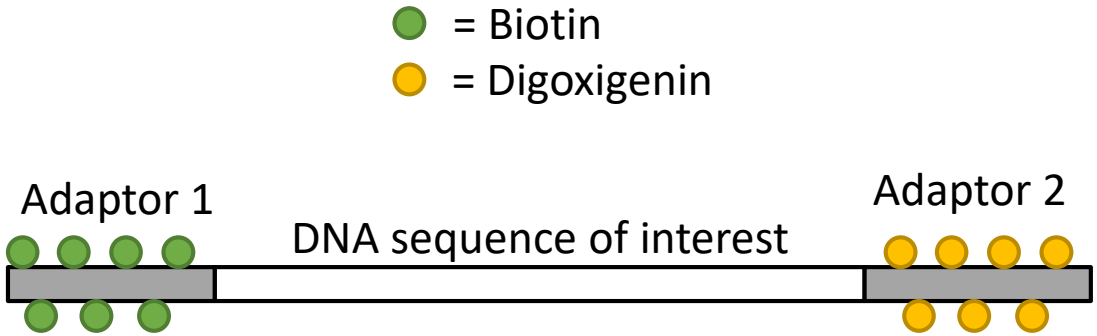
= Biotin
= Digoxigenin
Adaptor 1
DNA sequence of interest
Adaptor 2

Figure 5

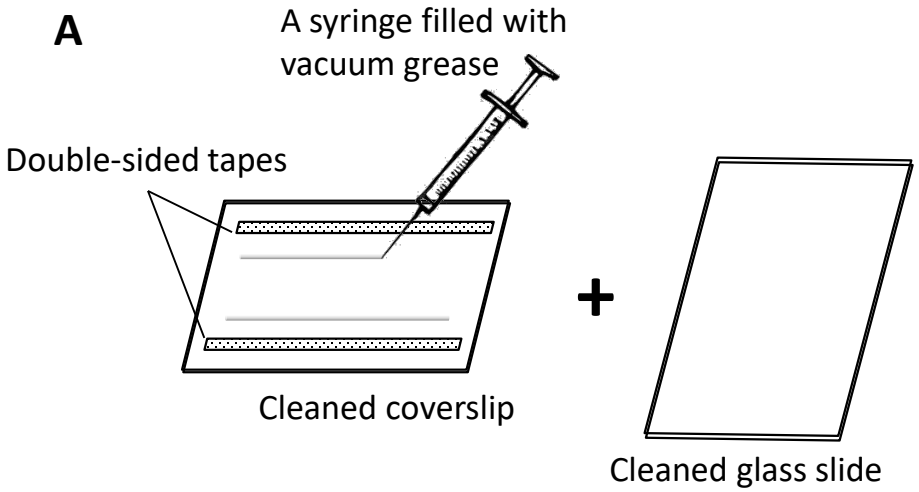
A
A syringe filled with
vacuum grease
Double-sided tapes
Cleaned coverslip
+
Cleaned glass slide

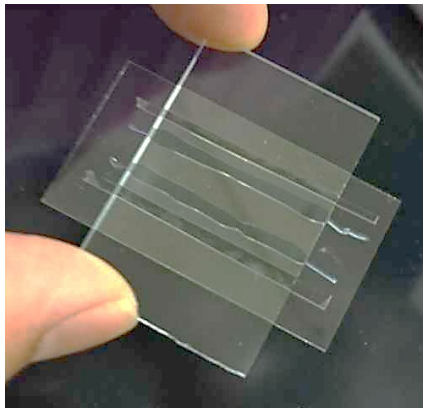
B

Figure 6

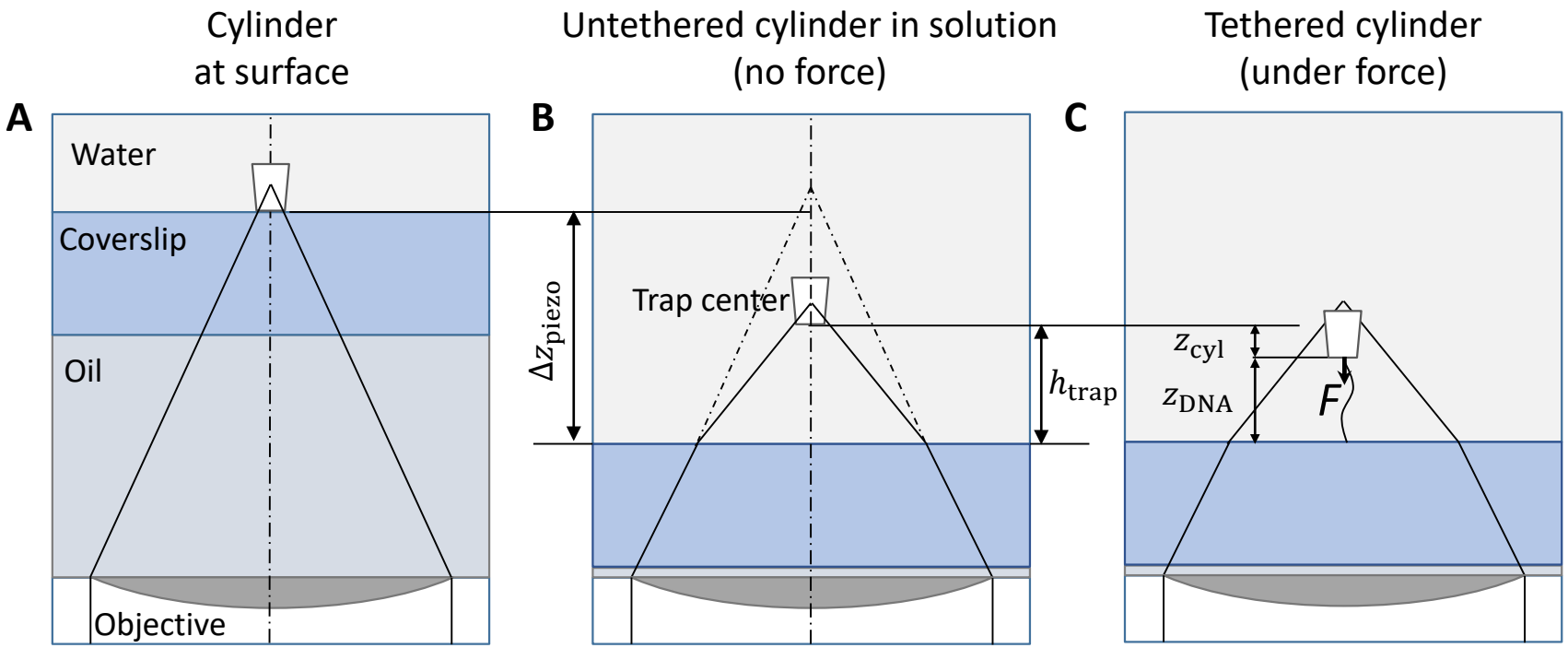
Cylinder
at surface
Untethered cylinder in solution
(no force)
Tethered cylinder
(under force)
A
B
C
Water
Coverslip
Oil
Objective
Trap center
$\Delta z_{\mathrm{piezo}}$
h_{trap}
z_{cyl}
z_{DNA}
F

Figure 7

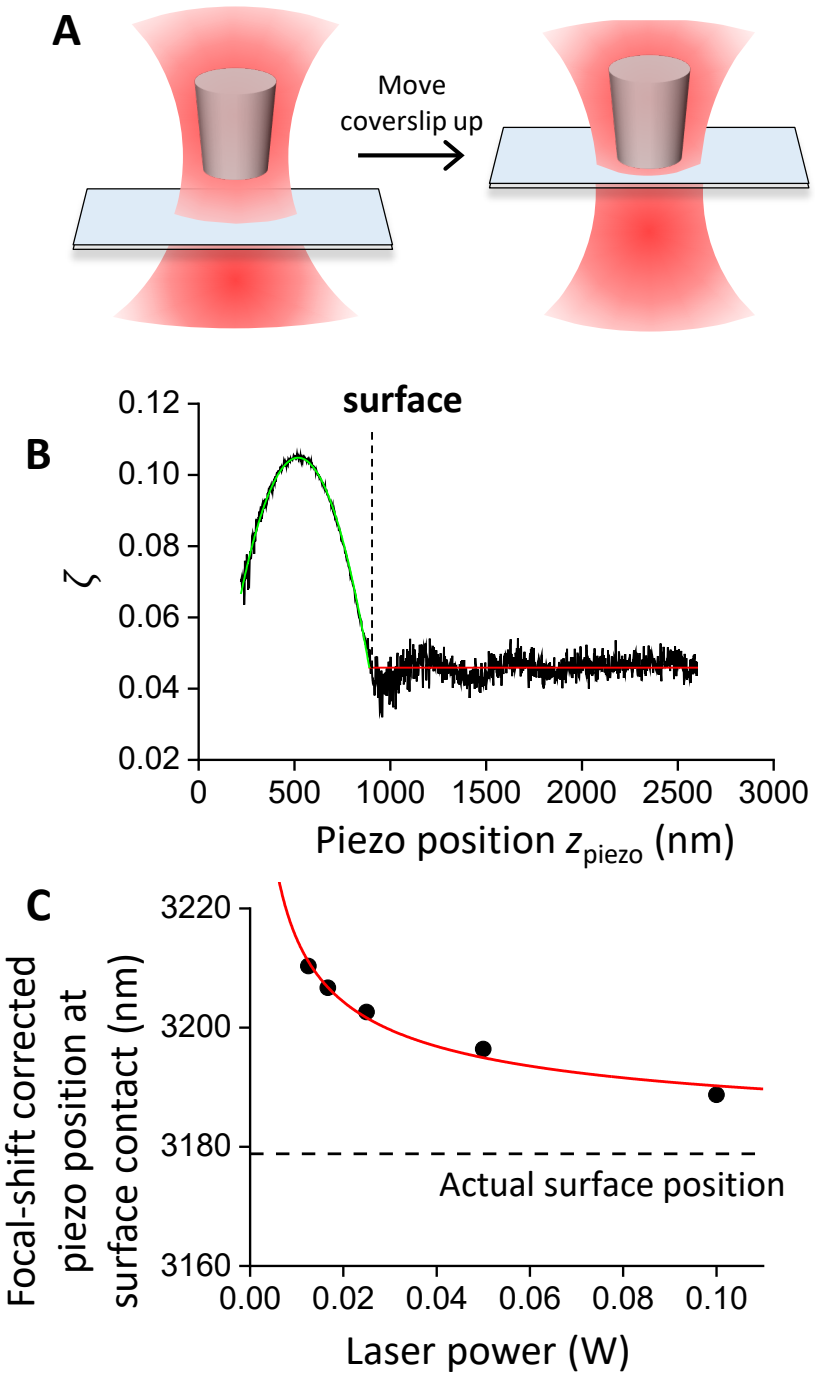
A
Move
coverslip up
B
surface
0.12
0.10
0.08
0.06
0.04
0.02
ζ
0
500
1000
1500
2000
2500
3000
Piezo position z_{piezo} (nm)
C
3220
3200
3180
3160
Actual surface position
Focal-shift corrected
piezo position at
surface contact (nm)
0.00
0.02
0.04
0.06
0.08
0.10
Laser power (W)

Figure 8

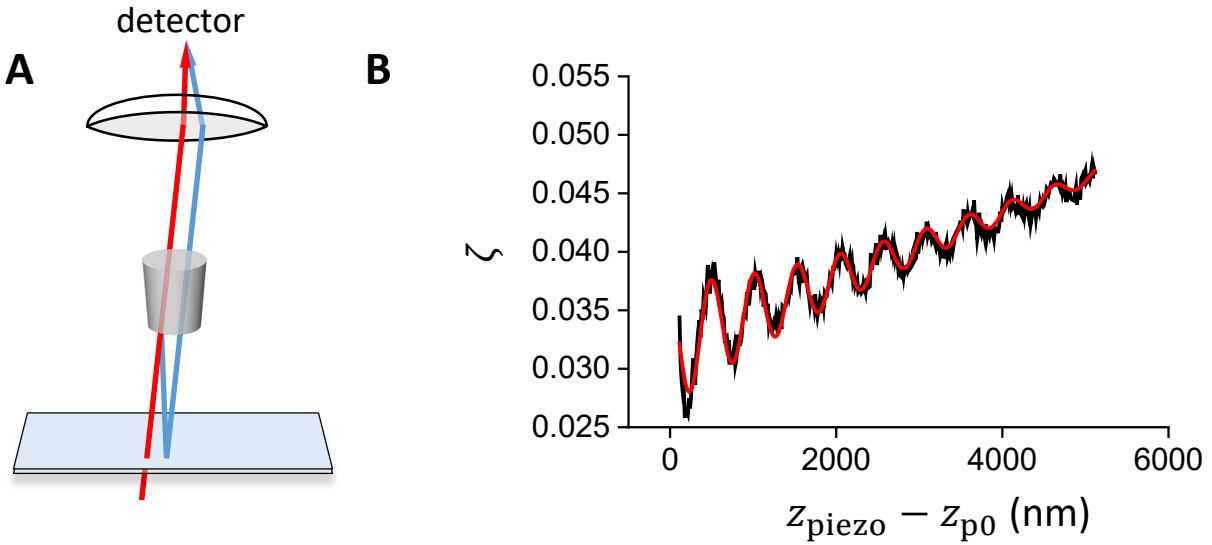
A
detector
B
0.055
0.050
0.045
0.040
0.035
0.030
0.025
ζ
0
2000
4000
6000
$z_{\mathrm{piezo}} - z_{\mathrm{p0}}$ (nm)

Figure 9

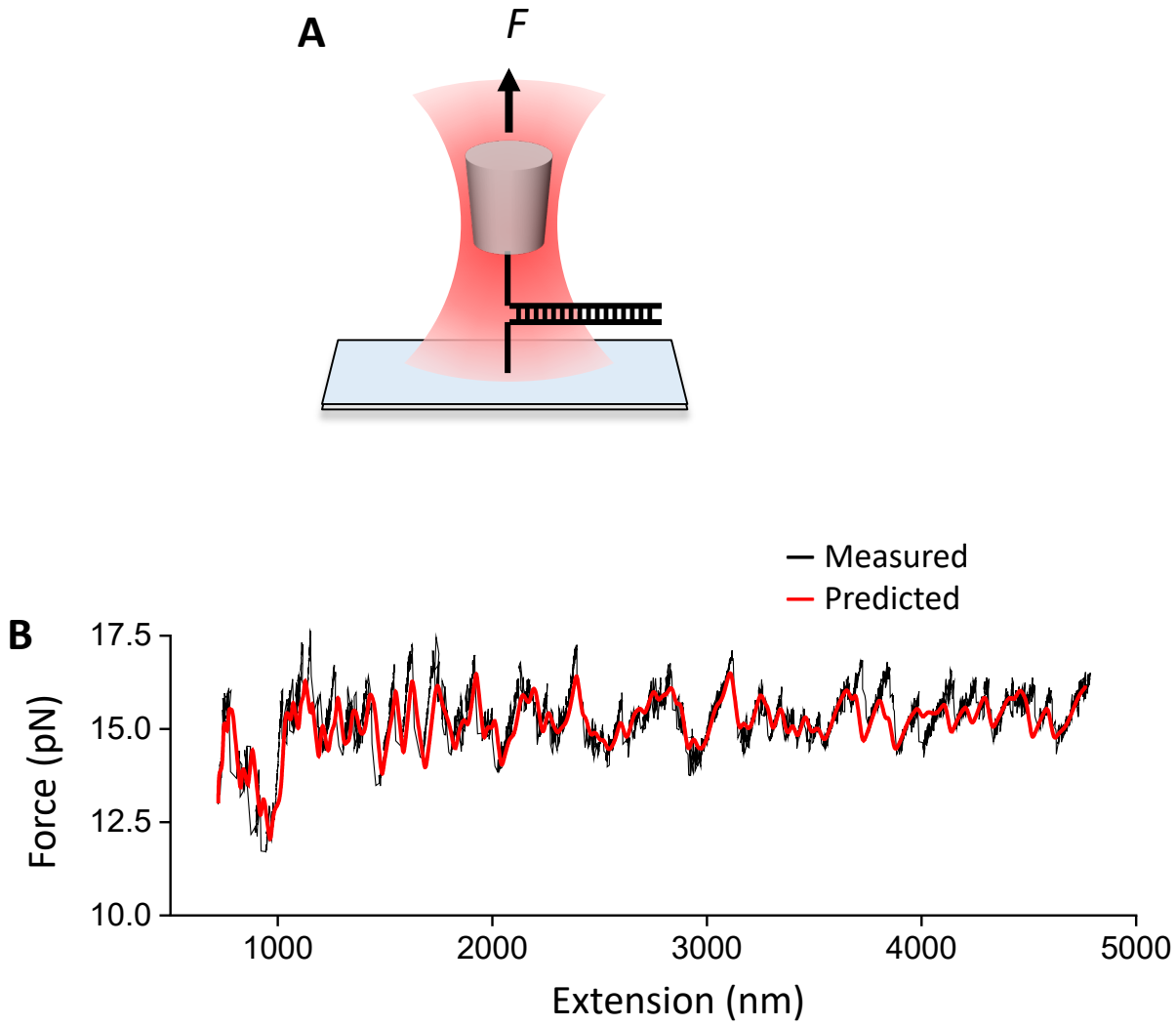
A
F
B
Measured
Predicted
17.5
15.0
12.5
10.0
Force (pN)
1000
2000
3000
4000
5000
Extension (nm)

Figure 10

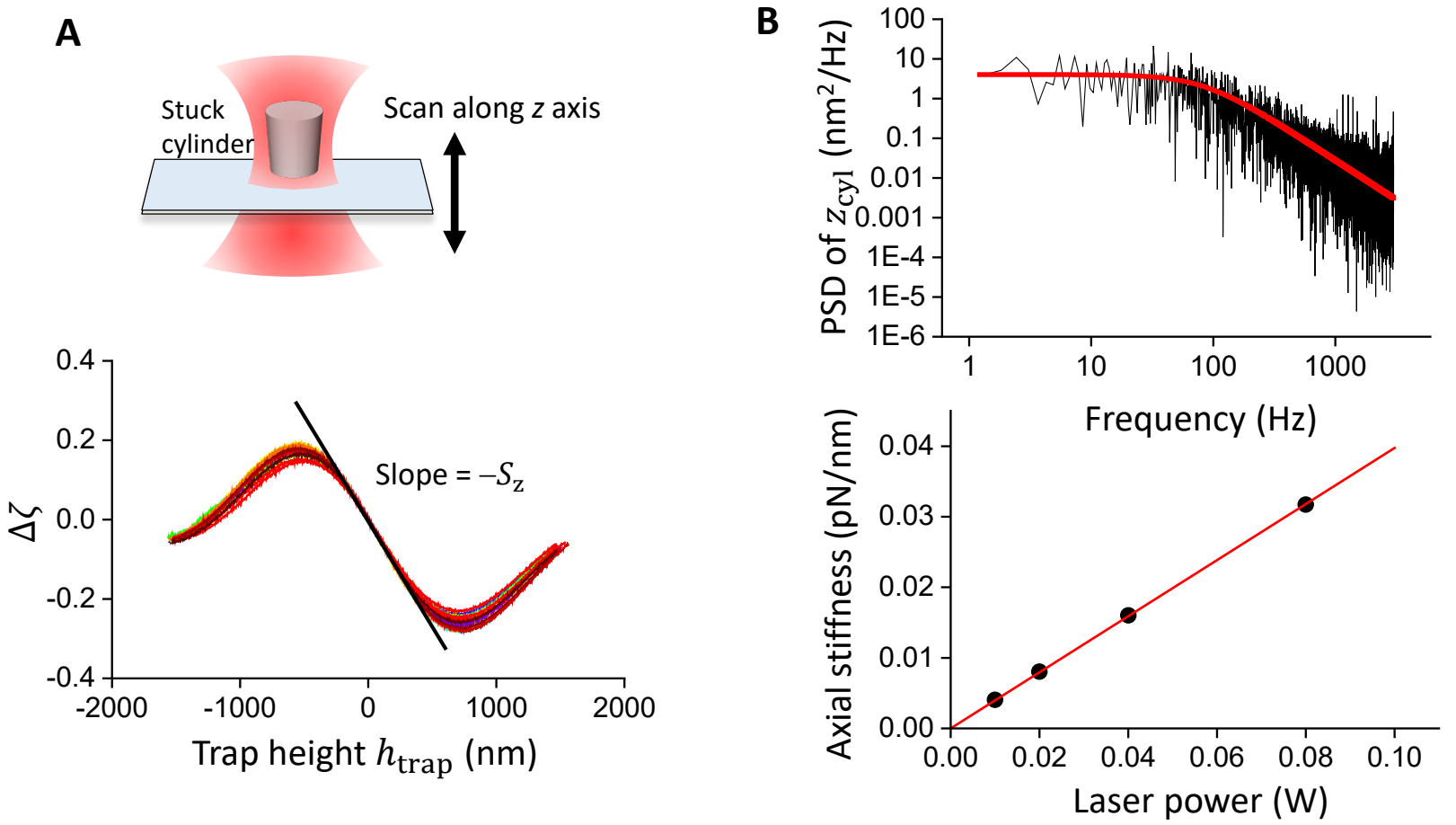
A
Stuck cylinder
Scan along z axis
0.4
0.2
0.0
-0.2
-0.4
Δζ
Slope = $-S_z$
-2000
-1000
0
1000
2000
Trap height h_{trap} (nm)
B
100
10
1
0.1
0.01
0.001
1E-4
1E-5
1E-6
PSD of z_{cyl} (nm²/Hz)
1
10
100
1000
Frequency (Hz)
0.04
0.03
0.02
0.01
0.00
Axial stiffness (pN/nm)
0.00
0.02
0.04
0.06
0.08
0.10
Laser power (W)

Figure 11

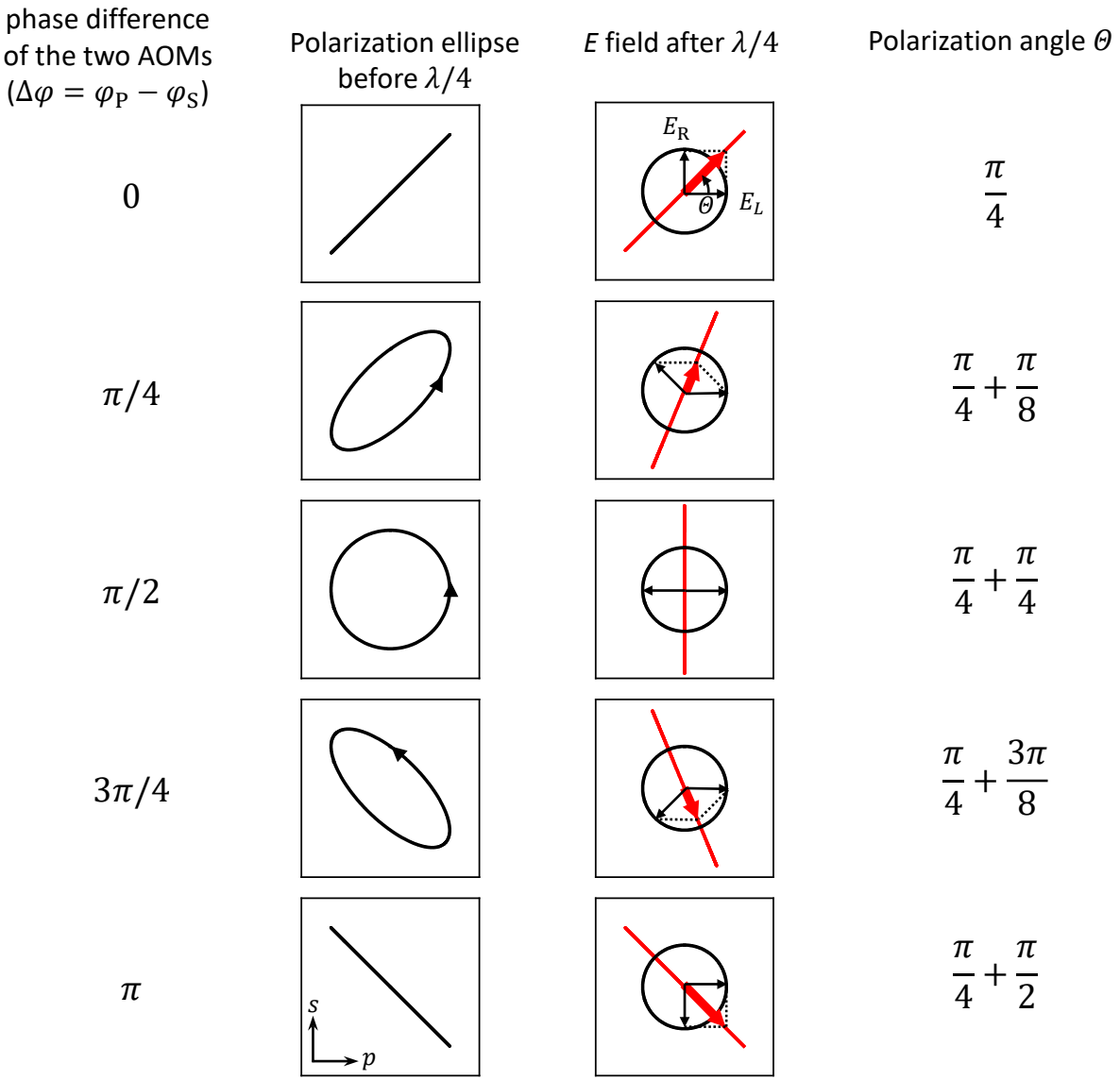
phase difference of the two AOMs ($\Delta\varphi = \varphi_P - \varphi_S$)
Polarization ellipse before $\lambda/4$
E field after $\lambda/4$
Polarization angle Θ
0
$\pi/4$
$\pi/2$
$3\pi/4$
π
E_R
E_L
Θ
s
p
$\frac{\pi}{4}$
$\frac{\pi}{4} + \frac{\pi}{8}$
$\frac{\pi}{4} + \frac{\pi}{4}$
$\frac{\pi}{4} + \frac{3\pi}{8}$
$\frac{\pi}{4} + \frac{\pi}{2}$

Figure 12

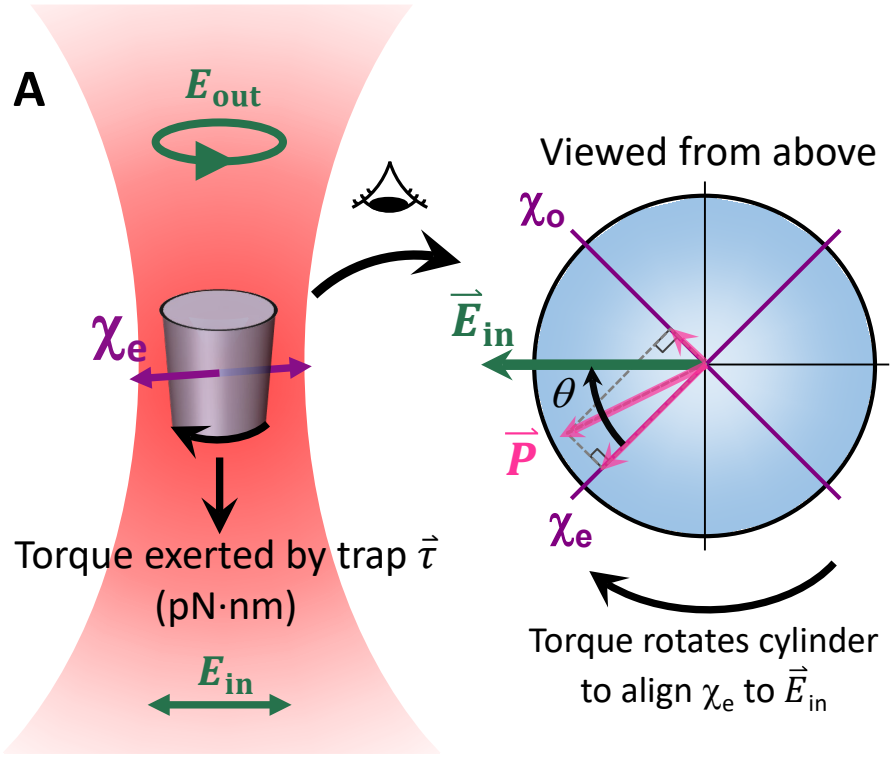
A
E_{out}
χ_e
Torque exerted by trap $\vec{\tau}$
(pN·nm)
E_{in}
Viewed from above
χ_o
$\vec{E}_{in}$
θ
$\vec{P}$
χ_e
Torque rotates cylinder
to align χ_e to $\vec{E}_{in}$

Figure 13

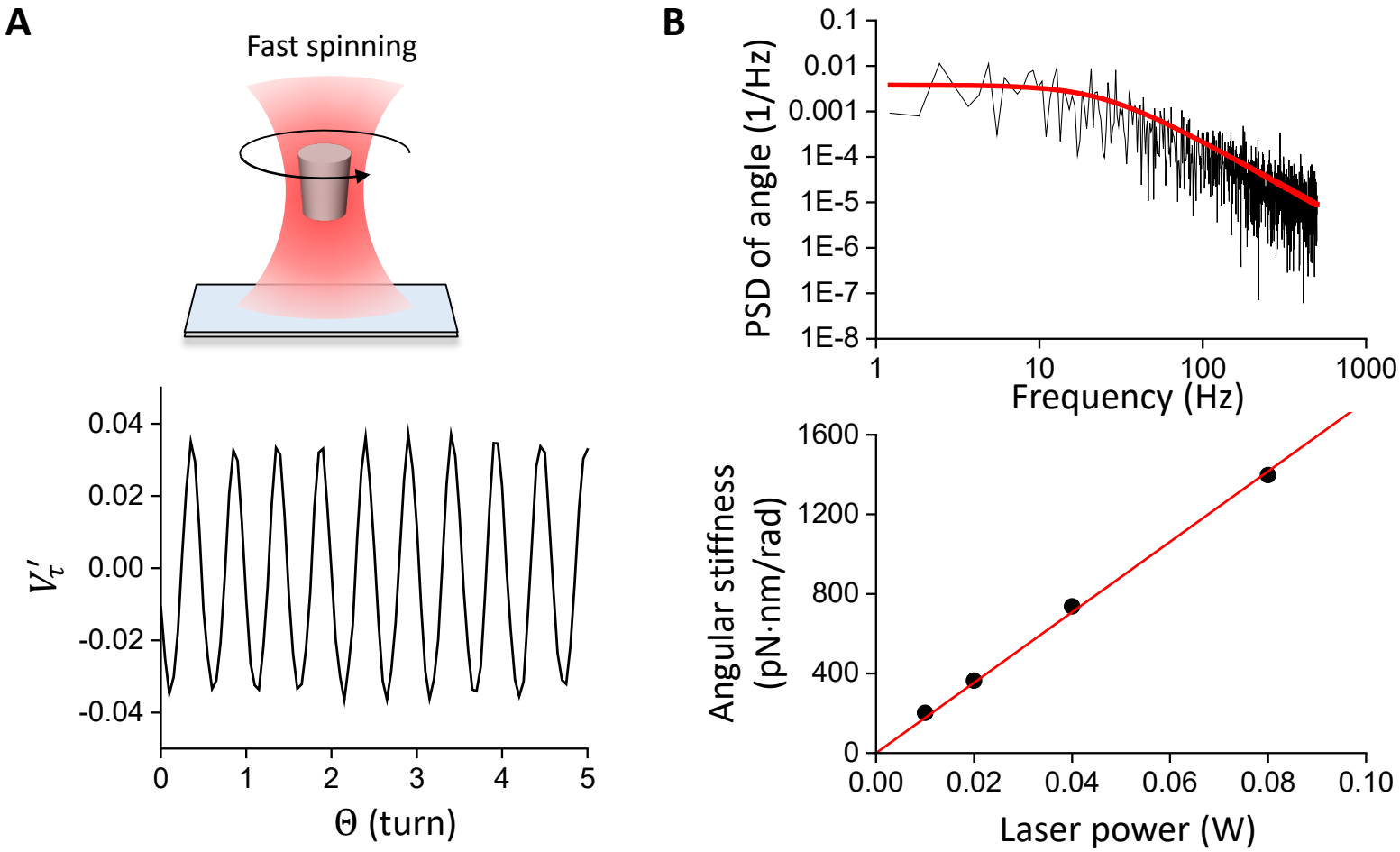
A
Fast spinning
0.04
0.02
0.00
-0.02
-0.04
V_τ'
0
1
2
3
4
5
Θ (turn)
B
0.1
0.01
0.001
1E-4
1E-5
1E-6
1E-7
1E-8
PSD of angle (1/Hz)
1
10
100
1000
Frequency (Hz)
1600
1200
800
400
0
Angular stiffness (pN·nm/rad)
0.00
0.02
0.04
0.06
0.08
0.10
Laser power (W)

Figure 14

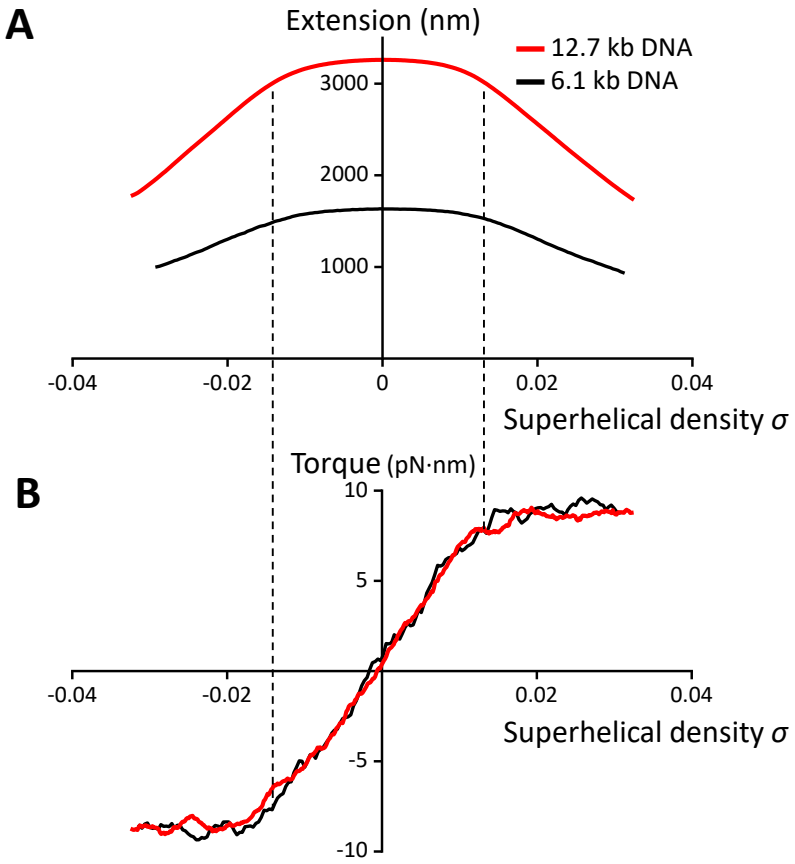
A
Extension (nm)
12.7 kb DNA
6.1 kb DNA
3000
2000
1000
-0.04
-0.02
0
0.02
0.04
Superhelical density σ
B
Torque (pN·nm)
10
5
-5
-10
-0.04
-0.02
0.02
0.04
Superhelical density σ

Figure 15

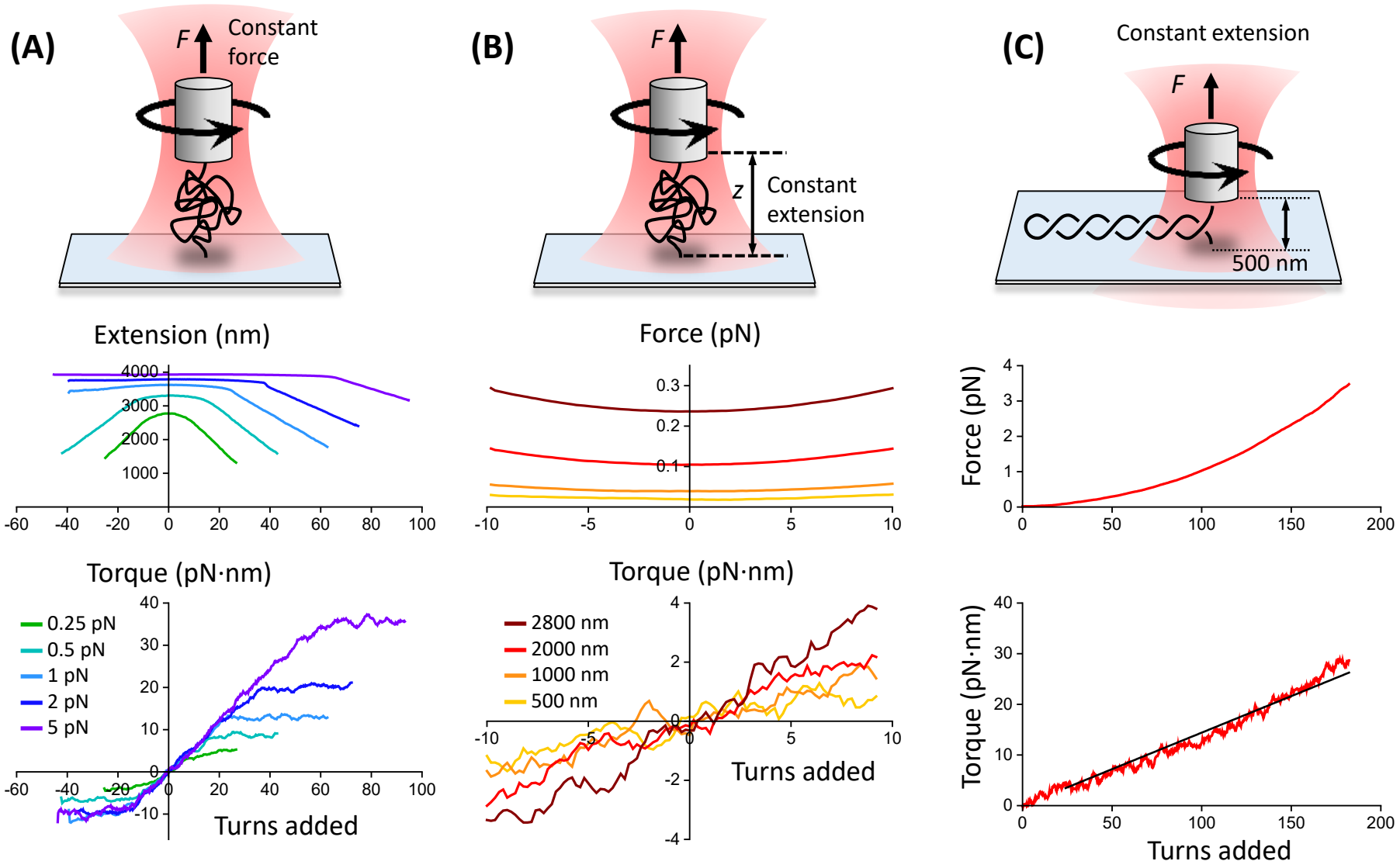
(A)
F
Constant force
Extension (nm)
4000
3000
2000
1000
-60 -40 -20 0 20 40 60 80 100
Torque (pN·nm)
0.25 pN
0.5 pN
1 pN
2 pN
5 pN
40 30 20 10 0 -10
-60 -40 -20 0 20 40 60 80 100
Turns added
(B)
F
z
Constant extension
Force (pN)
0.3
0.2
0.1
-10 -5 0 5 10
Torque (pN·nm)
2800 nm
2000 nm
1000 nm
500 nm
4 2 0 -2 -4
-10 -5 0 5 10
Turns added
(C)
Constant extension
F
500 nm
Force (pN)
4 3 2 1 0
0 50 100 150 200
Torque (pN·nm)
40 30 20 10 0
0 50 100 150 200
Turns added